

Revisiting the Fundamental Planes of Black Hole Activity for Strong Jet Sources

QING-CHEN. LONG ^{1,2} AI-JUN. Dong[†] ^{1,2} QIN-JUN. ZHI ^{1,2} AND LUN-HUA. SHANG ^{1,2}

¹*School of Physics and Electronic Science, Guizhou Normal University, Guiyang 550001, People's Republic of China; aijdong@gznu.edu.cn*

²*Guizhou Provincial Key Laboratory of Radio Astronomy and Data Processing, Guizhou Normal University, Guiyang 550001, People's Republic of China*

ABSTRACT

Whether the X-ray emissions of strong jet sources originate from disk+coronas or jets is still controversial. In this work, we constructed a strong jet sample containing 50 flat-spectrum radio quasars, 51 low-synchrotron-peaked BL Lac objects and 18 intermediate-synchrotron-peaked BL Lac objects to explore the origin of X-ray emissions. Generally, blazars are the typical radio-loud active galactic nucleus with a powerful jet toward the observer, causing their broadband emissions to be boosted. By considering the Doppler boosting effect, we obtain the intrinsic radio–X-ray correlation and the fundamental plane (FP) of black hole activity for the strong jet sources: the intrinsic radio–X-ray correlation is $L_{R,int} \propto L_{X,int}^{1.04}$, which favor the jet-dominated mode, the intrinsic FP is $\log L_{R,int} = (1.07 \pm 0.06) \log L_{X,int} - (0.22 \pm 0.10) \log M_{BH} - (3.77 \pm 2.11)$, which can be interpreted by the hybrid mode of jet+standard disk. Our results suggest that the X-ray emissions of strong jet sources are dominated by the jets, but there may also be a small contribution from the disk. In addition, the radio–X-ray correlation and FP of strong jet sources do not have a significant dependence on the Eddington-ratio.

Keywords: Accretion – Accretion disks: Black Hole Physics – Galaxy Nuclei: Jets and outflows – X-ray: Blazars – FSRQs and BL Lacs

1. INTRODUCTION

Active galactic nucleus (AGNs) are widely believed to be powered by an accreting supermassive black holes (SMBHs; $10^6-10^10 M_{\odot}$, e.g., Magorrian et al. 1998; Padovani et al. 2017). Understanding the accretion physics and feedback of AGNs has an important implication for insights into the growth and evolution of host galaxies (Blandford et al. 2019). There are two classification of AGNs are observationally distinguished by the radio-loudness parameter, $R = F_{5\text{GHz}}/F_{4400\text{\AA}}$, where $F_{5\text{GHz}}$ and $F_{4400\text{\AA}}$ are the rest-frame 5 GHz radio flux density and optical flux density at 4400 Å band, respectively (Kellermann et al. 1989). Only 10% – 20% of AGNs are radio-loud AGNs (RL-AGNs) with $R \geq 10$, while the rest are radio-quiet AGNs (RQ-AGNs) with $R < 10$ (Ivezić et al. 2002; Kellermann et al. 2016). Gen-

erally, RL-AGNs exhibit the powerful relativistic jets that are absent in RQ-AGNs (Padovani et al. 2017).

However, the RL-AGNs/RQ-AGNs dichotomy is often debated in previous studies. For example, (1) this dichotomy has been made along different criteria in previous works, e.g., most of works used $R_{\text{crit}} = 10$ as the criterion of this dichotomy; however, $R_{\text{crit}} = 17$ and $R_{\text{crit}} = 30$ were presented in Zhang et al. (2021) and Bariuan et al. (2022), respectively. (2) Brinkmann et al. (2000) and Bonchi et al. (2013) found that the RL-AGNs/RQ-AGNs dichotomy did not show a bimodal distribution. (3) R depend on the Eddington-ratio ($R \propto 1/\lambda_{\text{Edd}}$, see Ho 2002; Sikora et al. 2007; Broderick & Fender 2011), which was interpreted as a change in the accretion mode ($\lambda_{\text{Edd}} > 0.01$ corresponds to a radiatively efficient accretion, while the lower λ_{Edd} corresponds to a radiatively inefficient advection dominated accretion flow, i.e. ADAF. see Ho 2002), but Ballo et al. (2012) found R is not significantly correlated with λ_{Edd} . 3) Whether the RL-AGNs are the strong jet sources has been controversial (Meyer et al. 2011; Keenan et al. 2021).

It is generally accepted that the X-ray emissions of RL-AGNs mainly come from jets (Yuan et al. 2009; Wang et al. 2006; de Gasperin et al. 2011; Bariuan et al. 2022; Dong et al. 2023; Wang et al. 2024), but there are some views think the X-ray emissions of RL-AGNs come from the disk or corona (Li et al. 2008; Li & Gu 2018, 2021; Zhu et al. 2020). The fundamental plane (FP) of black hole activity can provide us with an opportunity to gain the insight into the accretion mode of various accreting BHs, as well as to constrain the origin of X-ray emissions (see the works of FP; Merloni et al. 2003; Falcke et al. 2004; Yuan & Cui 2005; Yuan et al. 2009; K rding et al. 2006; Wang et al. 2006; Li et al. 2008; G ltekin et al. 2009; de Gasperin et al. 2011; Plotkin et al. 2012; Dong et al. 2014; Dong & Wu 2015; Fan & Bai 2016; Xie & Yuan 2017; Li & Gu 2018; Liao et al. 2020; Bariuan et al. 2022; Wang et al. 2024; Zhang et al. 2024). Over the past 20 yr, the researches on FP have been well developed and refined, such as the FP is sensitive to the weight of adopted sample (K rding et al. 2006; Plotkin et al. 2012), the FP depends on the radio-loudness (Wang et al. 2006; Li et al. 2008; Bariuan et al. 2022; Wang et al. 2024) and the Eddington-ratio of X-ray luminosity ($\lambda_{\text{Edd}} = \log(L_X/L_{\text{Edd}})$, hereafter λ_{Edd} ; see Yuan & Cui 2005; Yuan et al. 2009; Dong & Wu 2015; Xie & Yuan 2017; Wang et al. 2024). However, the previous works that study the dependence of FP on λ_{Edd} only focus on the low-luminosity AGNs (LLAGNs); such studies are absent in the brighter blazars.

So far, there have been two different views on the FP and X-ray emissions' origin of RL-AGNs. The prevailing view thought that the FP of RL-AGNs is steeper than of RQ-AGNs, which is attributed to the fact that RL-AGNs are jet-dominated sources (see works of radio-loud sample, e.g., Yuan et al. 2009; Wang et al. 2006; Li et al. 2008; de Gasperin et al. 2011; Plotkin et al. 2012; Xie & Yuan 2017; Liao et al. 2020; Dong et al. 2021, 2023; Bariuan et al. 2022; Wang et al. 2024). However, an opposing view was proposed by Li & Gu (2018), who constructed a radio-loud sample that contains 13 low-excitation radio galaxies (LERGs) from *3CRR* catalog to study FP. They found a shallower radio-X-ray correlation ($L_R \propto L_X^{0.63}$) and FP ($\xi_X = 0.52$, $\xi_M = 0.84$), which are consistent with the ADAF mode, and they argued that the X-emissions come from the accretion flows rather than jets. In addition, Li & Gu (2021) firstly found a significant relationship between the mid-infrared to X-ray spectral index α_{IX} and the Eddington-ratio λ_{IR} ($\alpha_{\text{IX}} - \lambda_{\text{IR}}$; see their Figure 2) for a radio-loud sample, which is flatter than the $\alpha_{\text{OX}} - \lambda_{\text{O}}$ relationship in RQ-AGNs (Lusso et al. 2010), implied the disk origin of the X-ray emissions. A similar view has also been claimed

in Zhu et al. (2020), they found that the jet-linked component is only important for a fraction (< 10%) of flat-spectrum radio quasars (FSRQs), and the corona-linked component dominates the X-ray emissions of most RL-AGNs.

In the unified model of RL-AGNs, blazars are the typical RL-AGNs that present a powerful jet toward our line of sight (Urry & Padovani 1995), which causes their broadband emissions to be boosted. Blazars can be separated into two subclasses based on the equivalent width (EW) of the optical emission lines: FSRQs exhibit the strong emission lines ($\text{EW} > 5 \text{ \AA}$), while BL Lac objects have very weak or no emission lines ($\text{EW} < 5 \text{ \AA}$; e.g. Scarpa & Falomo 1997). In addition, the spectral energy distribution (SED) of blazars shows a double-hump structure, which are characterized by a synchrotron component at lower frequency hump and inverse Compton component at higher frequency hump (Fossati et al. 1998; Donato et al. 2001; Wu et al. 2007). Based on the location of synchrotron peak frequency ($\log \nu_{\text{peak}}$) in the SED, blazars are classified as low-synchrotron-peaked blazar (LSP; LBL for BL Lac objects), intermediate-synchrotron-peaked blazar (ISP; IBL for BL Lac objects) and high-synchrotron-peaked blazar (HSP; HBL for BL Lac objects). A reliable classification (see Fan et al. 2016) is given as the following: for LSP, $\log \nu_{\text{peak}} < 14$; for ISP, $14 < \log \nu_{\text{peak}} < 15.3$, and for HSP $\log \nu_{\text{peak}} > 15.3$. It is worth noting that FSRQs have almost no HSP (Fan et al. 2016; Ajello et al. 2022; Yang et al. 2022a). For the blazars' sequence, Meyer et al. (2011) and Keenan et al. (2021) have suggested that HBLs are the weak jet source, while the rest are the strong jet sources.

In this work, we compiled a strong jet sample from blazars' sequence to reexplore FP and X-ray emissions' origin of strong jet sources. This will help us resolve the possible controversies mentioned above and provide further insights into black hole accretion, jet formation, and feedback. Previous works have suggested that the strong jet blazars have a non-negligible Doppler beaming effect (Wu et al. 2007; Nieppola et al. 2008; Yang et al. 2022b). Therefore, the Doppler beaming effect should be taken into account for performing physical inference for mechanism of radiation. In addition, the studies of FP depending on λ_{Edd} are absent in the brighter blazars, we also examine whether the λ_{Edd} have a significant impact on FP of blazars. The structure of the paper is as follows. In §2, we detailedly describe our strong jet samples. In §3, we introduce data analysis and the fitting methods and present our best-fit results. The discussions and summaries of our results are presented in §4 and §5, respectively. For this paper, the cosmological

parameters are selected as $H_0 = 70 \text{ km s}^{-1} \text{ Mpc}^{-1}$, $\Omega_\Lambda = 0.73$, and $\Omega_M = 0.27$ (Dong & Wu 2015).

2. SAMPLE

Padovani & Giommi (1995) found that LBLs and HBLs occupy two completely different regions in the $\alpha_{\text{RO}} - \alpha_{\text{OX}}$ plane (see their Figure 12). In addition, the FSRQs and IBLs tend to inhabit in the similar region as LBLs rather than HBLs in the $\alpha_{\text{RO}} - \alpha_{\text{OX}}$ plane (detailedly see Figure 16, Figure 1, Figure 10, Figure 10 and Figure 6 in Donato et al. 2001; Padovani et al. 2003; Nieppola et al. 2006; Fan et al. 2016; Yang et al. 2022a, respectively), which indicates that the energy distribution of FSRQs, IBLs, and LBLs are closer to each other, while the energy distribution of HBLs is very different from them. Moreover, there are some evidences suggesting that the FSRQs, LBLs, and IBLs are strong jet sources that exhibit the radiatively efficient accretion, while the HBLs are weak jet sources that associated with ADAF mode (Meyer et al. 2011; Keenan et al. 2021, because the dichotomy between the strong jet sources and the weak jet sources does not belong to the scope of the discussion in this work, we refer the readers to the above paper for details of this classification). Besides, Donato et al. (2005) found that FSRQs and LBLs tracked the jet-dominated radio–X-ray correlation ($L_{\text{R}} \propto L_{\text{X}}^{1.06}$), while the HBLs have a shallower radio–X-ray correlation ($L_{\text{R}} \propto L_{\text{X}}^{0.64}$; see their Figure 4), which agree with ADAF mode in Merloni et al. (2003). Observationally, the very long baseline interferometry (VLBI) jets of HBLs appear in a plumelike morphology beyond a few milliarcseconds from the core, in contrast to the powerful jets of strong jet blazars that may remain well collimated to large distances (Piner et al. 2008). Therefore, we excluded the HBLs because we only focus on the strong jet sources.

To obtain the largest possible sample of strong jet source, we cross-referenced the FSRQs’ catalogue from (Hovatta et al. 2009), BL Lac objects’ catalog from Ye & Fan (2021) and Wu et al. (2014) with the synchrotron peak frequency $\log \nu_{\text{peak}}$ of Ajello et al. (2022) and Xiong et al. (2015). Besides, we also add five LBLs that were not used in their works, their 5 GHz core radio flux densities ($F_{\text{C},5\text{GHz}}$) taken from NED¹ or Yuan & Wang (2012), their 5 GHz Doppler factors δ are estimated by using Equation (6) in Ye & Fan (2021). In total, we have collected 50 FSRQs, 51 LBLs, and 18 IBLs for our strong jet sample; they have the available core radio flux density, X-ray flux density, BH mass, $\log \nu_{\text{peak}}$

and Doppler factor δ . It is noting that we focus only on the strong jet sources. Therefore, the radio-loudness R of blazars are calculated to ensure that they are all RL-AGNs, where the boundary of the radio-loudness dichotomy of $\log R = 1.23$ (ref Figure 6 in Zhang et al. 2021) is adopted in this work. In order to obtain the values of radio-loudness, we searched the optical flux densities at 4400 Å band in NED and CDS². For the sources without $F_{4400 \text{ Å}}$, the other optical bands are extrapolated to 4400 Å assuming a spectral index of $\alpha_o = -0.5$ ($F \propto \nu^\alpha$, see Bariuan et al. 2022).

2.1. The 5 GHz Core Radio Luminosity

In order to avoid the contamination from the star formation, in this paper, we use the core 5 GHz radio flux densities to calculate the 5 GHz core radio luminosities. For FSRQs, the $F_{\text{C},5\text{GHz}}$ were taken from NED or CDS. Because the strong jet blazars have the nonnegligible Doppler beaming effect, we taken the Doppler factor δ at 22 GHz and 37 GHz from Hovatta et al. (2009), which are extrapolated to the 5 GHz δ by using the empirical Equation (3) (detailedly see § 3.2). For LBLs and IBLs, their $F_{\text{C},5\text{GHz}}$ mainly come from Ye & Fan (2021) and Wu et al. (2014), the 5 GHz δ of their work are also adopted. But once the 5 GHz δ are taken from Ye & Fan (2021), the δ values that are estimated by using $q = 3 + \alpha$ ($\alpha = 0$) are adopted in this work (see their Equation (6)). The intrinsic radio luminosities are estimated by taking δ into account (detailedly see § 3.2).

2.2. The 2–10 keV X-Ray Luminosity

In this paper, the 2–10 keV X-ray Luminosities are calculated by using 2–10 keV X-ray flux densities ($F_{2-10 \text{ keV}}$). For our blazars, the X-ray observations are mainly detected by *Swift*, *Chandra* and *XMM-Newton*, their X-ray flux densities are taken from NED and the existing literatures. In order to minimize the observational errors, we preferred the X-ray data from *Chandra/XMM-Newton* if the source has the X-ray flux density that was detected by *Chandra/XMM-Newton*, owing to the *Chandra/XMM-Newton* have a higher spatial resolution. In addition, in order to avoid the errors caused by converting through another approximate wave band, we preferred the $F_{2-10 \text{ keV}}$. For the sources without the available $F_{2-10 \text{ keV}}$, the other approximate wavebands (e.g., 0.5–7 keV, 0.3–8 keV, 0.3–10 keV) are extrapolated to $F_{2-10 \text{ keV}}$ by using the available power law photon index Γ ($F_\nu \propto \nu^{1-\Gamma}$):

¹ <https://ned.ipac.caltech.edu/>

² <https://simbad.u-strasbg.fr/simbad/>

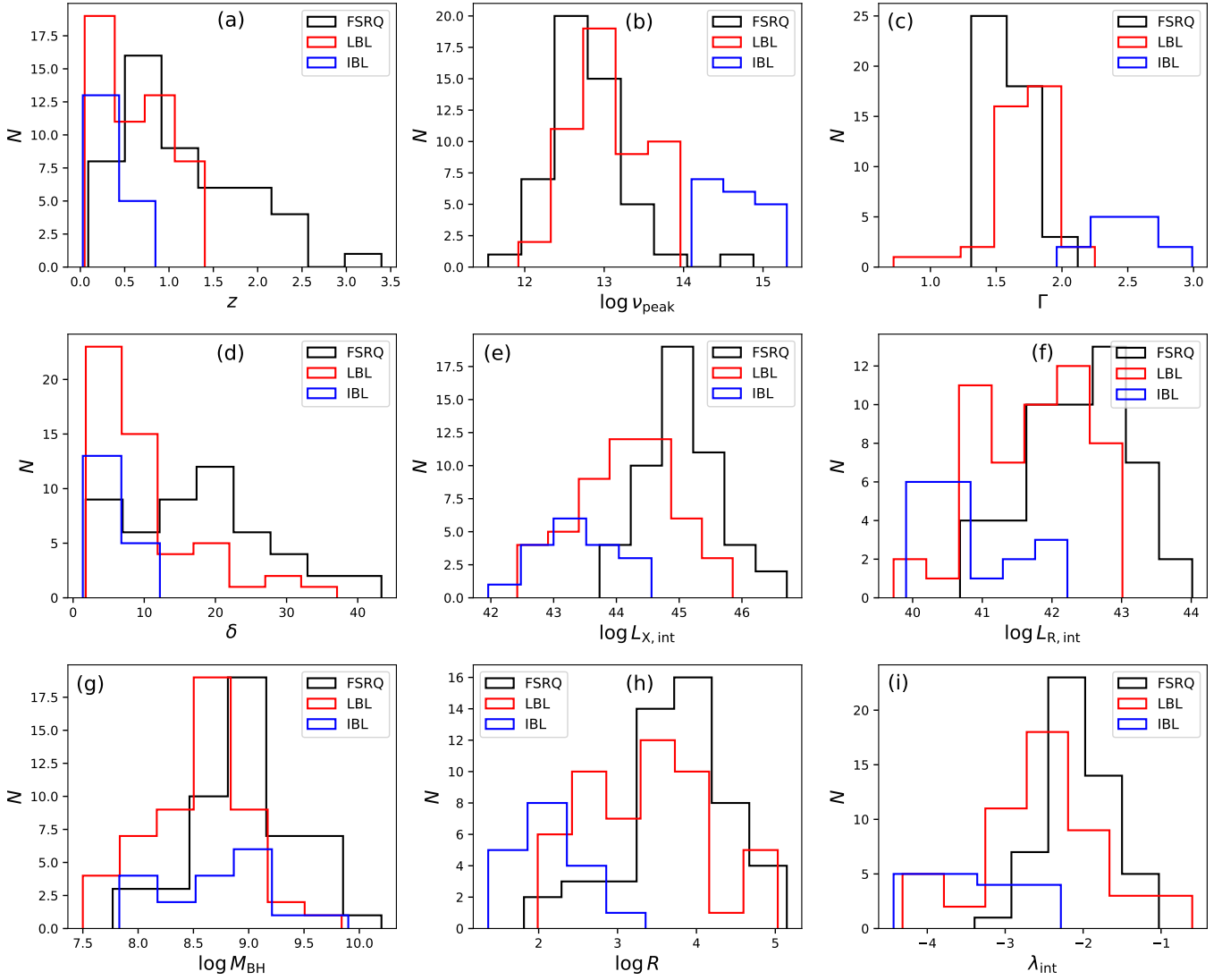


Figure 1. Distributions of the physical parameters for our samples, the black box, red box and blue box represent FSRQs, LBLs and IBLs, respectively. (a) Redshift: z , (b) Logarithm of the synchrotron peak frequency: $\log \nu_{\text{peak}}$, (c) The power law photon index: Γ , (d) The 5 GHz Doppler factor: δ , (e) Logarithm of the intrinsic X-ray luminosity at 2–10 keV band: $\log L_{X,\text{int}}$, (f) Logarithm of the intrinsic 5 GHz core radio luminosity: $\log L_{R,\text{int}}$, (g) Logarithm of the black hole mass: $\log M_{\text{BH}}$, (h) Logarithm of the radio-loudness: $\log R$, (i) Eddington-ratio: $\lambda_{\text{int}} = \log(L_{X,\text{int}}/L_{\text{Edd}})$.

$$F_{2-10\text{ keV}} = F_{a-b\text{ keV}} \frac{\int_a^b \nu^{1-\Gamma} d\nu}{\int_a^b \nu^{1-\Gamma} d\nu} \quad (1)$$

To reduce the errors caused by the Equation (1) and (2) ($q = 2 + \alpha_X = 1 + \Gamma$), the X-ray flux density and the power-law photon index Γ are taken from the same literature. For the sources without the simultaneous power-law photon index Γ , we adopt the average power-law photon index $\langle \Gamma \rangle$ that are averaged from the sources with the available power-law photon index: $\langle \Gamma \rangle = 1.58$ for FSRQs, $\langle \Gamma \rangle = 1.71$ for LBLs, $\langle \Gamma \rangle = 2.44$ for IBLs. Similarly, the intrinsic X-ray luminosities are estimated by using Equation (2).

2.3. The BH Mass

The BH mass (M_{BH}) of our blazars are searched in the existing literatures, and their BH mass have multiple estimates. The traditional virial BH mass is also known as the dynamical mass, which adopts an empirical relationship between the broad-line-region (BLR) size and the ionizing luminosity, as well as the measured broad-line width, assuming that the BLR clouds are gravitationally bound by the central BH. This method is usually applied to estimate the BH mass for FSRQs (e.g., Shen et al. 2011; Shaw et al. 2012). Because BL Lac objects have no or weak emission line, their BH mass are usually estimated from the properties of their host galaxies,

e.g., $M - \sigma$ and $M - L_{\text{bulge}}$ relations, where the σ and L_{bulge} are the stellar velocity dispersion and the bulge luminosity of the host galaxies, respectively. But there are some BL Lacs show the well-detected broad lines; their BH mass therefore are estimated by using the traditional virial method. The prioritization of the choice of BH mass is as follows: $M_{\text{virial}} > M - \sigma > M - L_{\text{bulge}}$. 0749 + 540 and 0642 + 449 do not have the dynamical mass available in the previous works, but we found the absolute magnitude $M_R = -24.8$ (Maselli et al. 2010) for 0749 + 540, then we used the $M - M_R$ relation from Wu et al. (2002) to estimate its M_{BH} ($\log M_{\text{BH}} = 8.94 M_{\odot}$). The BH mass of 0642 + 449 is $\log M_{\text{BH}} = 9.12 M_{\odot}$ that is obtained by combining the spectroscopic data from Torrealba et al. (2012) with Equation (2) of Shen et al. (2011). Finally, our basic data are listed in Table. 2 and Figure 1 shows some parameters' distribution of our sample.

3. DATA ANALYSIS AND RESULTS

3.1. The Doppler Boosting Effect for Blazars

Wu et al. (2007) and Nieppola et al. (2008) found an anticorrelation between the Doppler factor δ and $\log \nu_{\text{peak}}$ for the blazars with $\log \nu_{\text{peak}} < 15.3$ Hz, which was interpreted by Nieppola et al. (2008) in the framework that the lower $\log \nu_{\text{peak}}$ sources are being boosted more than higher $\log \nu_{\text{peak}}$ sources. Their results imply that the lower $\log \nu_{\text{peak}}$ blazars have more powerful jets than HBLs (i.e. $P_{\text{jet}} \propto \delta \propto 1/\log \nu_{\text{peak}}$). On the contrary, the HBLs show a horizontal line in $\delta - \log \nu_{\text{peak}}$ relation (see Figure 13 in Wu et al. 2007), which may be due to the fact that they are weak jet sources. In addition, the anticorrelation between luminosities and $\log \nu_{\text{peak}}$ (e.g., Fossati et al. 1998; Nieppola et al. 2006, 2008; Fan et al. 2016; Yang et al. 2022a,b) was also explained as the result of Doppler beaming effect.

Figure 2 (a)–(d) show the synchrotron peak frequency ($\log \nu_{\text{peak}}$) versus the 5 GHz Doppler factor (δ), radio-loudness ($\log R$), observational 5 GHz core radio luminosity ($\log L_{R,\text{obs}}$), and observational 2–10 keV X-ray luminosity ($\log L_{X,\text{obs}}$) for our sample, respectively. It is clear that all correlations above are negative. For Figure 2(a), which is consistent with results of Wu et al. (2007) and Nieppola et al. (2008) (see their Figure 13 and Figure 1, respectively). For Figure 2(b), to the best of our knowledge, this is the first study of the relationship between $\log \nu_{\text{peak}}$ and $\log R$. For Figure 2(c-d), which are consistent with the results of Nieppola et al. (2006), Fan et al. (2016), and Yang et al. (2022a). It is clear that the lower $\log \nu_{\text{peak}}$ sources have a larger δ , $\log R$, $L_{R,\text{obs}}$ and $L_{X,\text{obs}}$ (i.e., $1/\log \nu_{\text{peak}} \propto \delta \propto \log R \propto L_{R,\text{obs}} \propto L_{X,\text{obs}}$). It is noting that the X-ray

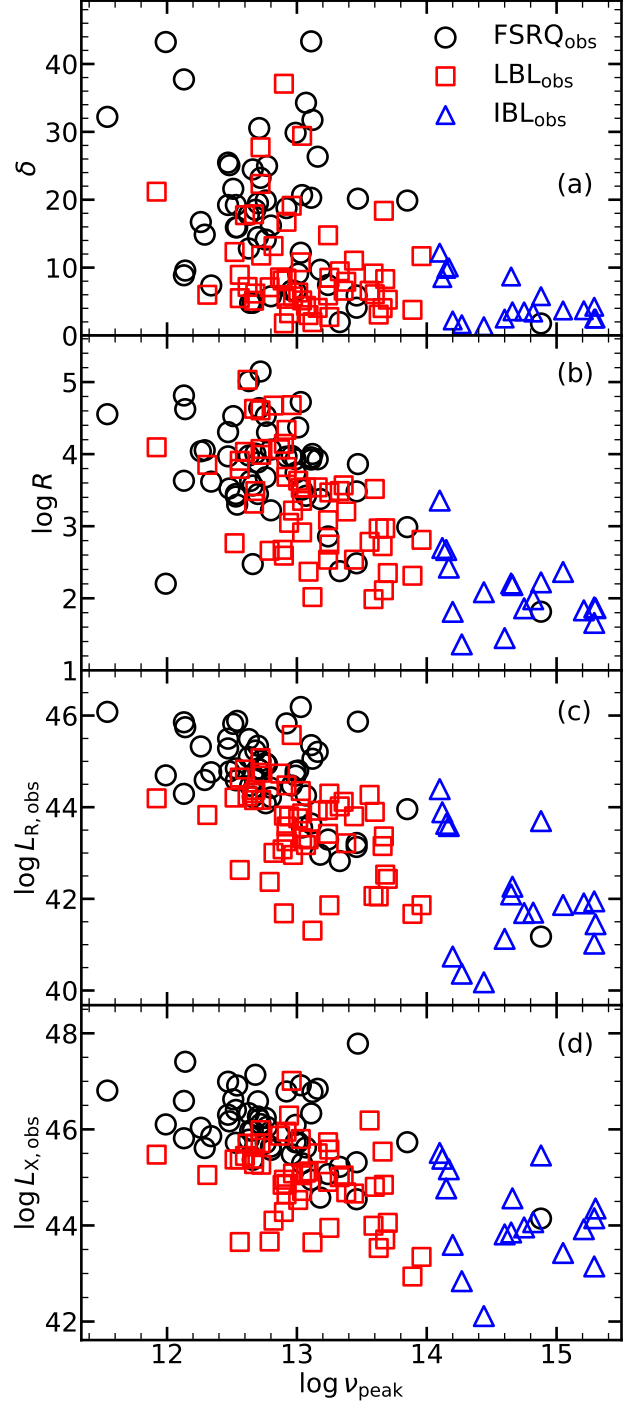


Figure 2. The (a)-(d) show the synchrotron peak frequency ($\log \nu_{\text{peak}}$) vs. the 5 GHz Doppler factor (δ), radio-loudness ($\log R$), observational 5 GHz core radio luminosity ($\log L_{R,\text{obs}}$), and 2–10 keV X-ray luminosity ($\log L_{X,\text{obs}}$), respectively. The black-circles, red-squares, and blue-triangles represent FSRQs, LBLs, and IBLs, respectively. The subscript "obs" or hollow-symbol denote the observational data.

emissions have a contribution of jets (synchrotron radiation or inverse Compton process). Therefore, the physical explanation for those anticorrelation is the boosted consequence of Doppler beaming effect, where the lower $\log \nu_{\text{peak}}$ sources have be more boosted, which causes a larger luminosity and radio-loudness (also see [Yang et al. 2022a](#)).

From the above theoretical analysis, we have again enough confidence to believe that our sample is a typical strong jet sample with a strong Doppler boosting effect. Therefore, the influence of Doppler boosting effect must be considered in our following radio–X-ray correlation and FP analysis.

3.2. Methods

It is clear that our sample has a strong beaming effect from the discussion and analysis in §3.1, the Doppler boosting effect therefore should be considered into the best fit of radio–X-ray correlation and the FP. In the beaming model, the observational flux density (F_{obs}) is strongly boosted from the intrinsic flux density (F_{int}):

$$F_{\nu,\text{int}} = F_{\nu,\text{obs}} \delta_{\nu}^{-q} \quad (2)$$

where the $F_{\nu,\text{int}}$, $F_{\nu,\text{obs}}$ are the intrinsic flux density and the observational flux density at ν band, respectively. $q = 2 + \alpha$ for the continuous jets, where α is the spectral index. For the radio band, the typical value of $\alpha_{\text{R}} = 0$ ([Donato et al. 2001](#); [Dong et al. 2023](#)) is adopted in this work, and the X-ray spectral indices are calculated using the $\alpha_{\text{X}} = \Gamma - 1$ ([Lusso et al. 2010](#)). Through Equation (2), we divided our data into ‘observational data bin’ and ‘intrinsic data bin.’

For 5 GHz radio Doppler factor (δ_{R}) of FSRQs and the 2–10 keV X-ray Doppler factor (δ_{X}) of all blazars, which are extrapolated from the Doppler factors at other frequencies by using the assumption that Doppler factor depend on the emission frequency ([Fan et al. 1994](#)), the form of equation is as follow:

$$\delta_{\nu} = \delta_{\text{o}}^{1 + \frac{1}{8} \log \frac{\nu_{\text{o}}}{\nu}} \quad (3)$$

where δ_{o} is the optical Doppler factor at the typical optical band of ν_{o} ($\log \nu_{\text{o}} = 14$ Hz, see [Fan et al. 1994](#)). The 5 GHz radio frequency and X-ray frequency at 2–10 keV band are $\log \nu_{\text{R}} = 9.7$ Hz and $\log \nu_{\text{X}} = 18.16$ Hz, respectively. Hence, we can get an equation of $\delta_{\text{X}} \approx \delta_{\text{R}}^{1/3}$. Similarly, the 22 GHz and 37 GHz δ of FSRQs ([Hovatta et al. 2009](#)) are also converted to the 5 GHz δ .

To reexplore the FP for strong jet sources, a similar method in [Merloni et al. \(2003\)](#) is adopted in this work, which has the form $\log L_{\text{R}} = \xi_{\text{X}} \log L_{\text{X}} + \xi_{\text{M}} \log M_{\text{BH}} + c_0$. In order to find the multivariate relation coefficients, we

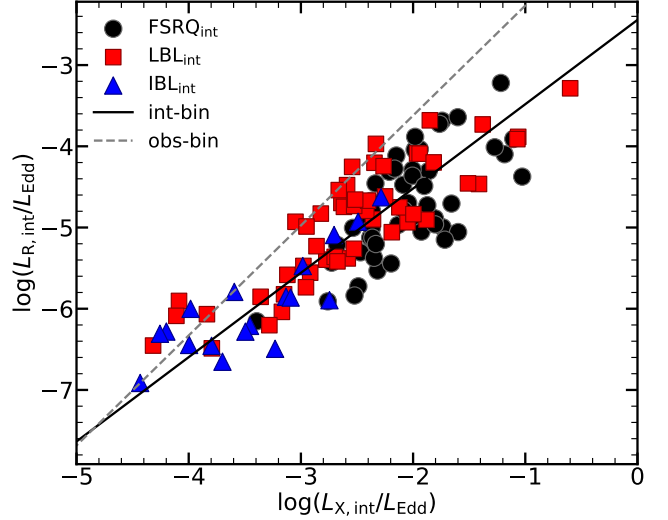


Figure 3. The Eddington-scaled radio–X-ray correlation. Similarly, the black-circles, red-squares and blue-triangles represent FSRQs, LBLs and IBLs, respectively. The subscript ‘int’ or solid-symbol denote the intrinsic data. The black solid line represent best-fit line of the intrinsic data bin, the gray dashed line represent best-fit line of the observational data bin.

adopt the least χ^2 approach in [Merloni et al. \(2003\)](#) and minimized the following statistic:

$$\chi^2 = \sum_i \frac{(y_i - c_0 - \xi_{\text{X}} X_i - \xi_{\text{M}} M_i)^2}{\sigma_{\text{R}}^2 + \xi_{\text{X}}^2 \sigma_{\text{X}}^2 + \xi_{\text{M}}^2 \sigma_{\text{M}}^2} \quad (4)$$

where the $y_i = \log L_{5\text{GHz}}$, $X_i = \log L_{2-10\text{keV}}$, $M_i = \log M_{\text{BH}}$ and c_0 is constant. For blazars, the uncertainties of the data mainly come from the nonsimultaneity between radio and X-ray emissions. Considering the systematic and the observed uncertainties, we adopt the typical isotropic uncertainties with $\sigma_{\text{R}} = \sigma_{\text{X}} = \sigma_{\text{M}} = 0.3$ dex, following [Merloni et al. \(2003\)](#) and [Xie & Yuan \(2017\)](#). Noticing, we used this approach to fit our intrinsic data bin and observational data bin, respectively.

3.3. Results

By considering the Doppler beaming effect, we obtain the observational and intrinsic radio–X-ray correlation for our strong jet blazars. Figure 3 shows our results, and their best fits are given as follows:

$$\log\left(\frac{L_{\text{R,obs}}}{L_{\text{Edd}}}\right) = (1.35 \pm 0.06) \log\left(\frac{L_{\text{X,obs}}}{L_{\text{Edd}}}\right) - (0.91 \pm 0.10) \quad (5)$$

with an intrinsic scatter of $\sigma_{\text{int}} = 0.42$ dex, a Spearman correlation coefficient of $R=0.89$ and $P = 2.02 \times 10^{-42}$.

$$\log\left(\frac{L_{\text{R,int}}}{L_{\text{Edd}}}\right) = (1.04 \pm 0.05) \log\left(\frac{L_{\text{X,int}}}{L_{\text{Edd}}}\right) - (2.44 \pm 0.14) \quad (6)$$

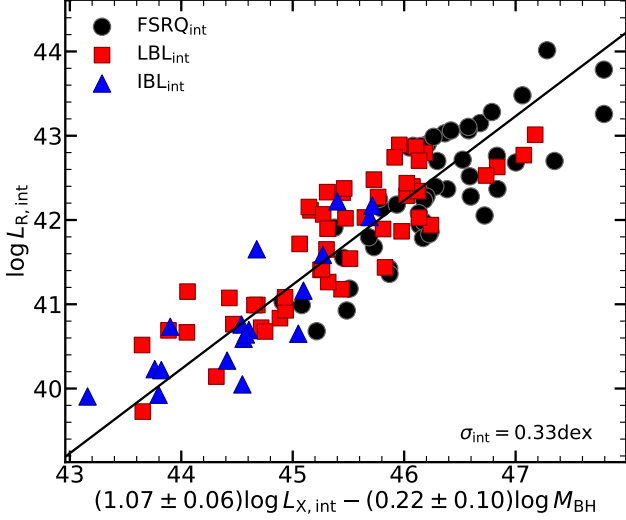


Figure 4. The FP_{int} for our strong jet sources, where the notations are the same as that of Figure 3.

with an intrinsic scatter of $\sigma_{\text{int}} = 0.32$ dex, a Spearman correlation coefficient of $R=0.82$ and $P = 1.43 \times 10^{-29}$.

The intrinsic radio–X-ray correlation is roughly consistent with the theoretical prediction of the pure jet-dominated mode ($L_R \propto L_X^{1.23}$, see Yuan & Cui 2005), while the Doppler beaming effect causes the observational radio–X-ray correlation to be steeper than the theoretical prediction above.

Through Equation (4), we obtain the observational FP (FP_{obs}) and the intrinsic FP (FP_{int} , see Figure 4) for the strong jet sources. Their best fits are given as follows:

$$\log L_{R,\text{obs}} = (1.39 \pm 0.06) \log L_{X,\text{obs}} - (0.34 \pm 0.12) \log M_{\text{BH}} - (15.98 \pm 2.18) \quad (7)$$

with a larger intrinsic scatter of $\sigma_{\text{int}} = 0.43$ dex.

$$\log L_{R,\text{int}} = (1.07 \pm 0.06) \log L_{X,\text{int}} - (0.22 \pm 0.10) \log M_{\text{BH}} - (3.77 \pm 2.11) \quad (8)$$

with an intrinsic scatter of $\sigma_{\text{int}} = 0.33$ dex.

We find that our FP_{int} is roughly consistent with the hybrid mode of jet+standard disk (SSD) in Bariuan et al. (2022) and Wang et al. (2024), while the FP_{obs} is close to the FP of RL-AGNs of Li et al. (2008) who attributed the steeper FP to the Doppler beaming effect.

Following Dong & Wu (2015), in order to reinvestigate the radio–X-ray correlation and eliminate the possible effect of mass, we further select a subsample with a narrow range of BH mass, which can simulate a single SMBH evolution for our strong jet sources. Finally, we selected 74 sources from table. 2, which have the BH

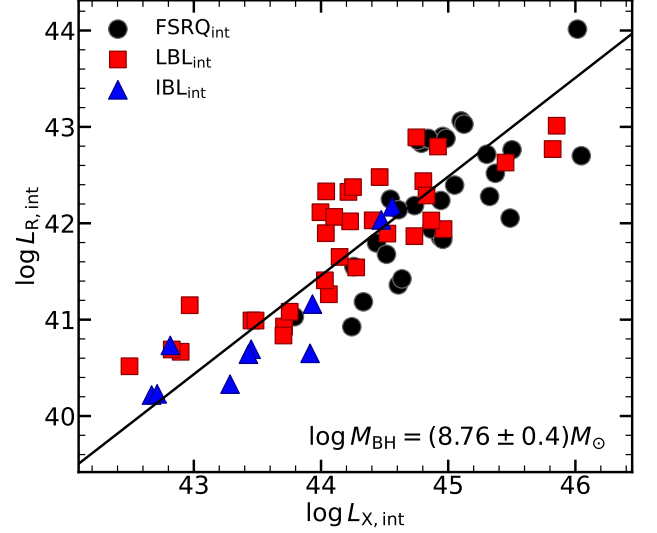


Figure 5. The relation between 5 GHz radio and 2–10 keV X-ray luminosity for strong jet subsample with BH mass $\log M_{\text{BH}} = (8.80 \pm 0.4) M_{\odot}$. The notations are the same as that of Figure 3. The black solid line is the best fit of intrinsic data bin for Single-BH subsample.

mass $\log M_{\text{BH}} = \log \bar{M}_{\text{BH}} \pm 0.4 = (8.76 \pm 0.4) M_{\odot}$ and the Eddington-ratio in a narrow range ($\lambda_{\text{int}} = -4.5 \sim -1$: which spans almost the entire range of our sample). The result is shown in Figure 5, the best-fit linear regression between the intrinsic radio luminosity and the X-ray luminosity for our single-BH sample is the following:

$$\log L_{R,\text{int}} = (1.03 \pm 0.07) \log L_{X,\text{int}} - (3.66 \pm 3.01) \quad (9)$$

with an intrinsic scatter of $\sigma_{\text{int}} = 0.34$ dex, a Spearman correlation coefficient of $R=0.82$ and $P = 5.07 \times 10^{-19}$, which is roughly consistent with Dong & Wu (2015) and Xie & Yuan (2017).

3.4. Correlation Tests

The Malmquist biases are ubiquitous in astronomical surveys, and mitigating these biases is vital to perform astrophysical inference. Therefore, the luminosity–luminosity correlations should be tested for the possible presence of a spurious correlation introduced by their common dependence on the distance (Merloni et al. 2003; Wang et al. 2006; Li et al. 2008). Different from their method, we perform the Spearman partial correlation analysis to test the correlation between luminosities, as well as between the Eddington-luminosity-scaled luminosities. For the given three variables (X , Y , Z), the partial correlation coefficient between X and Y , while keeping Z as the third variable, can be expressed as

$$R_{XY,Z} = \frac{R_{XY} - R_{XZ}R_{YZ}}{[(1 - R_{XZ}^2)(1 - R_{YZ}^2)]^{1/2}} \quad (10)$$

where the R_{XY} denotes the Spearman rank correlation coefficient between quantity X and Y , and so on. Table 1 shows the results of our test, namely, whether the correlation between X and Y is intrinsic or only introduced by a third variable Z . The null hypothesis will be rejected when its probability less than the significance level (i.e., 0.05).

For our correlations between luminosities, the same dependence on the distance always confuses the intrinsic physical relation. This is the main reason why Bregman (2005) thinks the FP is a distance artifact. The partial correlation analysis indeed proves that luminosities are still strongly correlated, even if the effect of distance is included. However, the significance level of radio–X-ray correlations becomes weaker when the distance is taken into account compared to BH mass. As in Wang et al. (2006), in order to avoid the distance effect, we test the existence of the intrinsic correlation between radio and X-ray emissions by comparing the radio and X-ray flux density. In Figure 6, we plot the 5 GHz radio flux density versus the 2–10 keV X-ray flux density. The observational and intrinsic radio–X-ray emissions are as follows:

$$\log F_{R,\text{obs}} = (1.60 \pm 0.16) \log F_{X,\text{obs}} + (5.58 \pm 1.95) \quad (11)$$

with an intrinsic scatter of $\sigma_{\text{int}} = 0.58$ dex, a Spearman correlation coefficient of $R=0.52$ and $P = 1.91 \times 10^{-9}$.

$$\log F_{R,\text{int}} = (1.06 \pm 0.09) \log F_{X,\text{int}} - (1.82 \pm 1.13) \quad (12)$$

with an intrinsic scatter of $\sigma_{\text{int}} = 0.33$ dex, a Spearman correlation coefficient of $R=0.62$ and $P = 3.53 \times 10^{-14}$.

It is clear that the correlation between radio and X-ray emissions of our sample really exists, even if the significance level has declined compared to the correlation between luminosities. However, the intrinsic scatter (σ_{int}) becomes smaller, and the significance level of radio–X-ray correlation becomes stronger when the Doppler factor is taken into account.

It can be found from the right panel of Figure 6 that the relation of $\log F_{R,\text{int}} - \log F_{X,\text{int}}$ of FSRQs, LBLs, and IBLs show three different intercepts. Considering jet-dominated X-ray and radio emissions, the radio and X-ray flux follows the scaling relation, which is obtained from Heinz (2004),

$$F_R \propto M_{\text{BH}}^{\frac{2p+13-(2+p)\alpha_R}{2p+8}} \dot{m}^{\frac{2p+13+(p+6)\alpha_R}{2(p+4)}} \quad (13)$$

$$F_X \propto M_{\text{BH}}^{(2-\alpha_X)/2} \dot{m}^{(5-3\alpha_X)/2} \quad (14)$$

where the p is the electron spectral index produced by the acceleration process (see Merloni et al. 2003; Heinz

2004). Combining Equation (13) with Equation (14), we can obtain the desired relation:

$$F_R \propto M_{\text{BH}}^{\frac{(2p+13-(2+p)\alpha_R)(p-1-\alpha_X)-2\alpha_R}{(p+4)(2p+1-3\alpha_X)}} F_X^{\frac{2p+13+(p+6)\alpha_R}{(p+4)(2p+1-3\alpha_X)}} \quad (15)$$

We can further get the relation of $\log F_R$ and $\log F_X$, that is,

$$\log F_R \propto \frac{2p+13+(p+6)\alpha_R}{(p+4)(2p+1-3\alpha_X)} \log F_X + \frac{(2p+13-(2+p)\alpha_R)(p-1-\alpha_X)-2\alpha_R}{(p+4)(2p+1-3\alpha_X)} \log M_{\text{BH}} \quad (16)$$

From Equation (16), the difference of intercepts for the three different classes of objects may be related to the BH mass, the electron spectral index, the radio spectral index, and the X-ray spectral index.

4. DISCUSSION

4.1. The Influence of Doppler Beaming Effect on Radio–X-Ray Correlation and FP

In some of the previous work studying FP of RL-AGNs (e.g., Wang et al. 2006; Li et al. 2008; Bariuan et al. 2022), their samples were doped with a few blazars, which may cause a spurious result. In this paper, we will emphasize the importance of considering the Doppler beaming effect for the strong jet blazars. It is well known that blazars have a nonnegligible Doppler beaming effect, especially for blazars with $\log \nu_{\text{peak}} < 15.3$, as confirmed in § 3.1. From Figure 3, Equation (7) and (8), we can find that the radio–X-ray correlation and FP become shallower by considering the Doppler beaming effect, which is consistent with Zhang et al. (2024). The plausible explanations are given as the following. On average, $\delta_{\text{FSRQs}} > \delta_{\text{LBLs}} > \delta_{\text{IBLs}}$ and $L_{\text{FSRQs}} > L_{\text{LBLs}} > L_{\text{IBLs}}$ (also see Figure 2, $\delta \propto L_R \propto L_X$), it is clear that a larger δ causes a larger boosting in luminosities (also see Nieppola et al. 2008; Yang et al. 2022a). Therefore, we can see that the gap between the black solid line and the gray dotted line in Figure 3 is getting bigger. Moreover, we also find the scatter of radio–X-ray correlation and FP get smaller by taking the Doppler factor into account. However, the significant level of observational radio–X-ray correlation is larger than that of intrinsic radio–X-ray correlation, which is due to the Doppler beaming effect and the distance effect stretching the range of luminosities. The significant level of intrinsic correlation between radio and X-ray emissions increases when eliminating the effect of distance (see Figure 6).

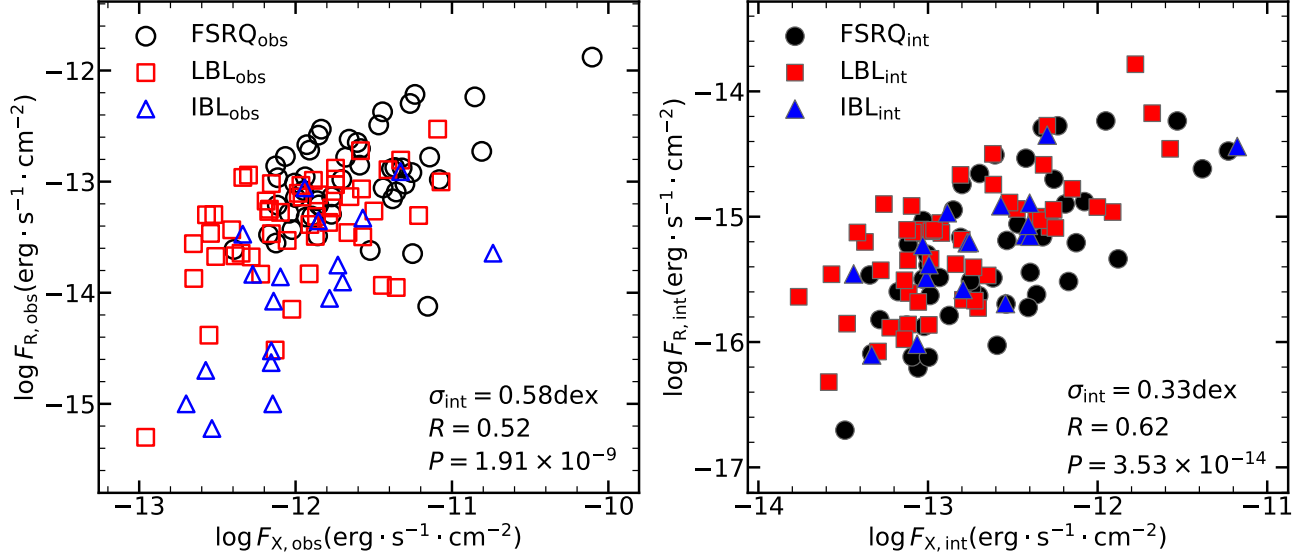


Figure 6. The left panel and right panel show the observational 5 GHz core radio flux densities vs. the observational 2–10 keV X-ray flux densities and the intrinsic 5 GHz core radio flux densities vs. the intrinsic 2–10 keV X-ray flux densities, respectively. The notations are the same as that of Figure 2 and Figure 3.

Table 1. The Spearman Partial Correlation Analysis

X	Y	Z	Number	$R_{XY,Z}$	P_{null}
$\log L_{X,\text{int}}$	$\log L_{R,\text{int}}$	$\log D$	119	0.58	6.99×10^{-12}
$\log(L_{X,\text{int}}/L_{\text{Edd}})$	$\log(L_{R,\text{int}}/L_{\text{Edd}})$	$\log D$	119	0.73	4.28×10^{-21}
$\log L_{X,\text{int}}$	$\log L_{R,\text{int}}$	None	119	0.89	3.02×10^{-42}
$\log L_{X,\text{int}}$	$\log L_{R,\text{int}}$	$\log M_{\text{BH}}$	119	0.86	7.96×10^{-35}
$\log(L_{X,\text{int}}/L_{\text{Edd}})$	$\log(L_{R,\text{int}}/L_{\text{Edd}})$	$\log M_{\text{BH}}$	119	0.86	7.96×10^{-35}

NOTE—Col (1): Variable X . Col (2): Variable Y . Col (3): Variable Z . Col (4): Number of the sources. Col (5): The partial correlation coefficient $R_{XY,Z}$. Col (6): The probability of null hypothesis P_{null} .

There is a noteworthy issue here, the Doppler factor is an unobserved quantity, and our Doppler factors are estimated by different method in the different literatures (see Hovatta et al. 2009; Wu et al. 2014; Ye & Fan 2021). However, we predict this does not have a significant effect on our results, owing to the anticorrelation between the Doppler factor and $\log \nu_{\text{peak}}$ intrinsically exist even if the Doppler factors are calculated in same method (Wu et al. 2007; Nieppola et al. 2008; Yang et al. 2022b). Therefore, our results are consistent with the theoretical expectations rather than the results being accidental.

4.2. A Significant Impact of Eddington luminosity ratios on Radio–X-Ray Correlation and FP for the Strong Jet Sources?

Previous works have suggested that the radio–X-ray correlation and FP depend on λ_{Edd} (see Yuan & Cui 2005; Yuan et al. 2009; Dong et al. 2014; Xie & Yuan

2017; Wang et al. 2024), which was interpreted as the transition of accretion mode (e.g., $\lambda_{\text{Edd}} < -6$ for jet-dominated mode, $-6 < \lambda_{\text{Edd}} < -3$ for ADAF mode, $\lambda_{\text{Edd}} > -3$ for disk mode). However, their works mainly focus on the LLAGNs instead of brighter blazars. Therefore, we want to examine whether the radio–X-ray correlation and FP of our blazars have a significant dependence on λ_{Edd} . However, our blazar sample has a relatively narrow range in the Eddington-ratio (see Figure 1 (i)), which will not allow us to divide our sample into several subsample with a narrower range of λ_{Edd} . Because, for the linear regression statistics, within the narrower range of λ_{Edd} , the radio–X-ray correlations and FP will produce erroneous slopes; we suggest that the range of λ_{Edd} should be larger than 3. Before performing the discussion, we need to emphasize that previous works have demonstrated that our

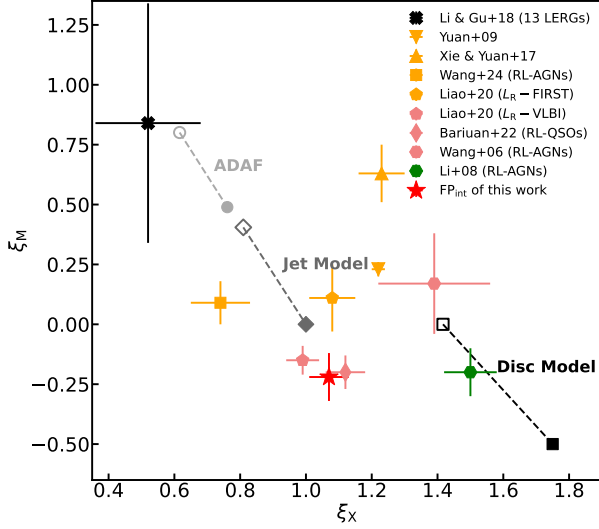


Figure 7. A comparison the best-fit correlation coefficients ξ_X and ξ_M of FP for radio-loud samples, include several previous works and this work. The black-cross is FP of RL-AGNs (13 LERGs) in Li & Gu (2018). The orange inverted-triangle, orange triangle, orange square, and orange pentagon are FP of Yuan et al. (2009), FP of Xie & Yuan (2017), FP_{RL-AGNs} of Wang et al. (2024), and FP_{FIRST} of Liao et al. (2020), respectively. Note where the $L_R - VLBI$ and $L_R - FIRST$ represent the core radio emissions taken from VLBI and FIRST observation, respectively. The light-red pentagon, light-red diamond, and light-red hexagon are FP_{VLBI} of Liao et al. (2020), FP_{RL-QSOs} of Bariuan et al. (2022), and FP_{RL-AGNs} of Wang et al. (2006), respectively. The green hexagon is FP_{RL-AGNs} of Li et al. (2008). The red star is intrinsic FP (FP_{int}) in this work. In addition, the gray-circles, dark-gray diamonds, and black squares represent the theoretically predicted correlation coefficients of ADAF, jet, and disk mode from Merloni et al. (2003), respectively. Empty symbols are results for a radio spectral index $\alpha_R = 0$ and filled symbols for $\alpha_R = 0.5$, and three dashed lines represent different possible correlation coefficients due to variations of radio emission.

blazars ($\log \nu_{\text{peak}} < 15.3$) are strong jet sources that exhibit the radiatively efficient accretion (Meyer et al. 2011; Keenan et al. 2021). Therefore, they should favor the jet-dominated mode within the theoretical expectation. As expected, our sources tightly traced the jet-dominated mode and do not show a significant bias along the whole track (see Figure 3, 4, 5 and 6). Statistically, by considering the Doppler beaming effect, we find that our intrinsic correlations have a small scatter ($\sigma_{\text{int}} \leq 0.34$) and a relative good significant level. Those evidences above imply the radio-X-ray correlation and FP of our strong jet sources do not have a significant dependence on λ_{Edd} .

4.3. The FP and X-Ray Emissions' Origin of Strong Jet Sources

Theoretically, the collimated relativistic jets are produced from the innermost regions of the accretion disk, meaning that jet variables depend on the accretion rate (\dot{M}), and the scaled correlation was given by Heinz & Sunyaev (2003)

$$L_R \propto \dot{M}^{1.4} \quad (17)$$

In addition, the X-ray emissions are widely believed come from the inverse Compton scatter of soft photons and the form of the X-ray depends on \dot{M} as the following:

$$L_X \propto \dot{M}^q \quad (18)$$

Therefore, the correlation of radio-X-ray can be written as

$$L_R \propto L_X^{1.4/q} \quad (19)$$

where q value is corresponding to different mode; $q = 2.3$, $q = 1$ and $q = 1.1$ can be adopted for the radiative inefficiency flow (Merloni et al. 2003), the radiative efficiency flow (Dong et al. 2014) and a jet-dominated mode (Yuan & Cui 2005), respectively.

Our intrinsic radio-X-ray correlation ($L_{R,\text{int}} \propto L_{X,\text{int}}^{1.04}$) favors the jet-dominated mode in Yuan & Cui (2005), which implies that the X-ray emissions of strong jet sources mainly come from jets. For observational radio-X-ray correlation ($L_{R,\text{obs}} \propto L_{X,\text{obs}}^{1.35}$; the black dashed line in Figure 3), which is steeper than the pure jet-dominated mode ($L_R \propto L_X^{1.23}$), the physical reason may be that there is an extra contribution from the Doppler beaming effect. In addition, our result (see Figure 5) simulating the evolution of a single-BH for the strong jet sources still follows the jet-dominated mode (see Dong & Wu 2015; Xie & Yuan 2017), which further strengthens the conclusions of the present work.

The measured correlation coefficients (ξ_X , ξ_M) from FP can provide insight into the different emission mechanisms within the BHs, where the ratio of these observables corresponds to the predicted values from different emission modes (Merloni et al. 2003; Plotkin et al. 2012). In order to reexplore and refine the FP and X-ray emissions' origin of RL-AGNs, we plotted the $\xi_X - \xi_M$ diagram of FP of previous radio-loud works and this work in the parameter space of best-fit correlation coefficient (see Figure 7). We now classify accretion physics for FP of all radio-loud samples according to the $\xi_X - \xi_M$ cartoon diagram in Wang et al. (2024), detailedly see their Figure 6. Combining our Figure 7 with their Figure 6, we can find that the FP of Li & Gu (2018) are consistent with ADAF mode in Merloni et al. (2003). The FP of Wang et al. (2024), Xie & Yuan (2017), Yuan et al. (2009) and FP_{FIRST} in Liao et al. (2020) agree with the

pure jet-dominated mode in Yuan & Cui (2005), while the FP of Wang et al. (2006), Bariuan et al. (2022), FP_{VLBI} in Liao et al. (2020) and our FP_{int} favor the hybrid mode of jet+SSD (but the contribution of jets is probably bigger). The FP of Li et al. (2008) are located in the region of Disk mode, Li et al. (2008) thought the X-ray emissions of RL-AGNs come from accretion disk (support disk mode), and the reason for steeper FP is due to the Doppler beaming effect. Here, our FP_{obs} are close to their FP, but it is clear that the Doppler beaming effect causes FP_{obs} to bias the disk mode. Because our strong jet blazars have a $\log \nu_{peak} < 15.3$, according to the SED (Fossati et al. 1998; Donato et al. 2001), their X-ray emissions should come from the synchrotron emission tail or inverse Compton emissions in jet (also see Nieppola et al. 2006; Wu et al. 2007, 2014; Fan et al. 2016; Yang et al. 2022a). Therefore, it is difficult for us to circumvent the X-ray emissions come from the jets. To sum up, the most plausible explanation for our FP_{obs} is simply the joint result of jet-dominated flow and the Doppler beaming effect.

For the FP of Li & Gu (2018), their LERGs samples are RL-AGNs but still consistent with ADAF mode instead of jet-dominated mode. The best physical explanation is that LERGs are weak jet sources and dominated by radiatively inefficient accretion flows (Hardcastle et al. 2007; Meyer et al. 2011; Keenan et al. 2021). Therefore, the radio-loud source is not necessarily a strong jet source. So care must be taken when placing RL-AGNs on FP (also see Hardcastle et al. 2009).

4.4. The Dependence of FP on the BH Mass

From Figure 3, it can be found that the slope of the radio–X-ray correlation ξ_X is 1.04. Considering the BH mass, we can obtain the FP, where the $\xi_X \sim 1.07$ (see Figure 4). The above results suggest that the BH mass has a weak influence on the FP. Additionally, the $\xi_M \sim -0.22$ of FP_{int}, which is similar to that of Wang et al. (2006), Yuan et al. (2009), Liao et al. (2020) and Bariuan et al. (2022), also imply the BH mass has a weak influence on the FP and roughly agree with the theoretical prediction of jet-dominated mode ($0 \leq \xi_M \leq 0.41$: see Figure 7). To test this, we perform the partial correlation analysis by taking the BH mass into account (see table. 1). From table. 1, we can find that the correlation coefficient ($R_{XY,Z}$) between $\log L_{R,int}$ and $\log L_{X,int}$ only decreases from 0.89 to 0.86, which implies the our FP is not sensitive to the BH mass. Furthermore, we analyze the BH mass dependence of ADAF and SSD mode; Merloni et al. (2003) and Li & Gu (2018) found the radiatively inefficient FP with the $\xi_M \sim 0.78$ and $\xi_M \sim 0.84$, respectively,

which roughly agree with the theoretical prediction of ADAF mode ($0.49 \leq \xi_M \leq 0.80$) in Figure 7, suggesting that the ADAF mode has a strong dependence on BH mass. Dong et al. (2014) and Li et al. (2008) found the radiatively efficient FP with the $\xi_M \sim -0.22$ and $\xi_M \sim -0.20$, respectively, which are consistent with the theoretical prediction of SSD mode ($-0.50 \leq \xi_M \leq 0$) in Figure 7, suggesting that the SSD mode has a weak dependence on BH mass. Therefore, a possibly reasonable interpretation is that the BH mass dependence of FP is regulated by the accretion mode.

5. SUMMARY

It is widely believed that the X-ray emissions of strong jet sources (e.g., RL-AGNs and Blazars) mainly from the nonthermal emission in relativistic jets, but it is still controversial. Currently, there are two opposite views for this issue; a popular view (Körding et al. 2006; de Gasperin et al. 2011; Plotkin et al. 2012; Liao et al. 2020; Dong et al. 2021, 2023; Bariuan et al. 2022; Wang et al. 2024) supports the jet-dominated mode in Yuan & Cui (2005); ones are opposite (Li & Gu 2018, 2021) that favor the ADAF mode. Motivated by these issues, we constructed a strong jet blazar sample including 50 FSRQs, 51 LBLs and 18 IBLs to study the radio–X-ray correlation and the FP. Previous studies have suggested the radio–X-ray correlation and FP depend on λ_{Edd} but they mainly focus on general sources (e.g. LLAGNs); such studies are absent in bright blazars. Moreover, we take the Doppler factor into account due to the fact that our strong jet blazars have a nonnegligible Doppler beaming effect. Our main results can be summarized as the following:

(1) By considering the Doppler beaming effect, we find the intrinsic radio–X-ray correlation of strong jet sources is $L_{R,int} \propto L_{X,int}^{1.04}$, which favor the jet-dominated mode. This correlation remains even after removing the effect of distance, suggesting that the X-ray emissions of strong jet sources mainly come from jets. In addition, the simulation of the evolution of a single strong jet BH is still following the jet-dominated trace, which further strengthens our conclusions. The observational radio–X-ray correlation ($L_{R,obs} \propto L_{X,obs}^{1.35}$) suggests that the steeper slope may be due to the extra contribution from the Doppler beaming effect.

(2) Similarly, we obtain the FP_{int} by considering the Doppler beaming effect: $\log L_{R,int} = (1.07 \pm 0.06) \log L_{X,int} - (0.22 \pm 0.10) \log M_{BH} - (3.77 \pm 2.11)$, which is interpreted by the hybrid mode of jet+SSD, implying that the X-ray emissions of strong jet sources are dominated by jets, but there may also be a small contribution from the disk.

(3) Our sources tightly traced the jet-dominated mode and do not show a significant bias along the whole track. In statistics, the intrinsic correlations have a small scatter ($\sigma_{\text{int}} \leq 0.34$) and a relatively good significant level. Those evidences above imply the radio–X-ray correlation and FP of our strong jet sources have not a significant dependence on λ_{Edd} . The plausible reason is that our blazars are the strong jet sources; thus, they should favor the jet-dominated mode in the theoretical analysis.

ACKNOWLEDGEMENTS

This work is supported by the NSFC (12363005, 2022SKA0130104), the Foundation of Guizhou Provincial Education Department ((2020)003, QJHKYZ[2021]296), the Scientific Research Project of the Guizhou Provincial Education (KY[2022]132, KY[2022]137), Major Science and Technology Program of Xinjiang Uygur Autonomous Region (2022A03013-4) and the Science and the Technology Foundation of Guizhou Province (Nos. ZK[2022]304, QKHJC[2020]1Y018).

REFERENCES

- Abdo, A. A., Ackermann, M., Ajello, M., et al. 2010, *ApJ*, 716, 835, doi: [10.1088/0004-637X/716/1/835](https://doi.org/10.1088/0004-637X/716/1/835)
- Acciari, V. A., Aliu, E., Aune, T., et al. 2009, *ApJ*, 707, 612, doi: [10.1088/0004-637X/707/1/612](https://doi.org/10.1088/0004-637X/707/1/612)
- Acosta-Pulido, J. A., Agudo, I., Barrena, R., et al. 2010, *A&A*, 519, A5, doi: [10.1051/0004-6361/200913953](https://doi.org/10.1051/0004-6361/200913953)
- Ajello, M., Baldini, L., Ballet, J., et al. 2022, *ApJS*, 263, 24, doi: [10.3847/1538-4365/ac9523](https://doi.org/10.3847/1538-4365/ac9523)
- Aleksić, J., Alvarez, E. A., Antonelli, L. A., et al. 2012, *A&A*, 544, A142, doi: [10.1051/0004-6361/201219133](https://doi.org/10.1051/0004-6361/201219133)
- Ballo, L., Heras, F. J. H., Barcons, X., & Carrera, F. J. 2012, *A&A*, 545, A66, doi: [10.1051/0004-6361/201117464](https://doi.org/10.1051/0004-6361/201117464)
- Bariuan, L. G. C., Snios, B., Sobolewska, M., Siemiginowska, A., & Schwartz, D. A. 2022, *MNRAS*, 513, 4673, doi: [10.1093/mnras/stac1153](https://doi.org/10.1093/mnras/stac1153)
- Bhattacharya, D., Misra, R., Rao, A. R., & Sreekumar, P. 2013, *MNRAS*, 431, 1618, doi: [10.1093/mnras/stt281](https://doi.org/10.1093/mnras/stt281)
- Blandford, R., Meier, D., & Readhead, A. 2019, *ARA&A*, 57, 467, doi: [10.1146/annurev-astro-081817-051948](https://doi.org/10.1146/annurev-astro-081817-051948)
- Boissay, R., Ricci, C., & Paltani, S. 2016, *A&A*, 588, A70, doi: [10.1051/0004-6361/201526982](https://doi.org/10.1051/0004-6361/201526982)
- Bonchi, A., La Franca, F., Melini, G., Bongiorno, A., & Fiore, F. 2013, *MNRAS*, 429, 1970, doi: [10.1093/mnras/sts456](https://doi.org/10.1093/mnras/sts456)
- Bregman, J. N. 2005, arXiv e-prints, astro, doi: [10.48550/arXiv.astro-ph/0511368](https://doi.org/10.48550/arXiv.astro-ph/0511368)
- Brinkmann, W., Laurent-Muehleisen, S. A., Voges, W., et al. 2000, *A&A*, 356, 445
- Broderick, J. W., & Fender, R. P. 2011, *MNRAS*, 417, 184, doi: [10.1111/j.1365-2966.2011.19060.x](https://doi.org/10.1111/j.1365-2966.2011.19060.x)
- Carangelo, N., Falomo, R., Kotilainen, J., Treves, A., & Ulrich, M. H. 2003, *A&A*, 412, 651, doi: [10.1051/0004-6361:20031519](https://doi.org/10.1051/0004-6361:20031519)
- Carrera, F. J., Ebrero, J., Mateos, S., et al. 2007, *A&A*, 469, 27, doi: [10.1051/0004-6361:20066271](https://doi.org/10.1051/0004-6361:20066271)
- Cerruti, M., Ponti, G., Boisson, C., et al. 2011, *A&A*, 535, A113, doi: [10.1051/0004-6361/201116444](https://doi.org/10.1051/0004-6361/201116444)
- de Gasperin, F., Merloni, A., Sell, P., et al. 2011, *MNRAS*, 415, 2910, doi: [10.1111/j.1365-2966.2011.18904.x](https://doi.org/10.1111/j.1365-2966.2011.18904.x)
- Donato, D., Ghisellini, G., Tagliaferri, G., & Fossati, G. 2001, *A&A*, 375, 739, doi: [10.1051/0004-6361:20010675](https://doi.org/10.1051/0004-6361:20010675)
- Donato, D., Sambruna, R. M., & Gliozzi, M. 2005, *A&A*, 433, 1163, doi: [10.1051/0004-6361:20034555](https://doi.org/10.1051/0004-6361:20034555)
- Dong, A.-J., Du, B.-W., Liu, C., et al. 2023, *AN*, 344, e20230037, doi: [10.1002/asna.20230037](https://doi.org/10.1002/asna.20230037)
- Dong, A.-J., Ge, K., Liu, X., & Zhi, Q.-J. 2021, *AN*, 342, 191, doi: [10.1002/asna.202113903](https://doi.org/10.1002/asna.202113903)
- Dong, A.-J., & Wu, Q. 2015, *MNRAS*, 453, 3447, doi: [10.1093/mnras/stv1801](https://doi.org/10.1093/mnras/stv1801)
- Dong, A.-J., Wu, Q., & Cao, X.-F. 2014, *ApJL*, 787, L20, doi: [10.1088/2041-8205/787/2/L20](https://doi.org/10.1088/2041-8205/787/2/L20)
- Dwelly, T., Salvato, M., Merloni, A., et al. 2017, *MNRAS*, 469, 1065, doi: [10.1093/mnras/stx864](https://doi.org/10.1093/mnras/stx864)
- Falcke, H., Körding, E., & Markoff, S. 2004, *A&A*, 414, 895, doi: [10.1051/0004-6361:20031683](https://doi.org/10.1051/0004-6361:20031683)
- Fan, J. H., Huang, Z. H., Li, J. J., Xie, G. Z., & Zhang, J. Y. 1994, *Ap&SS*, 213, 305, doi: [10.1007/BF00658217](https://doi.org/10.1007/BF00658217)
- Fan, J. H., Yang, J. H., Liu, Y., et al. 2016, *ApJS*, 226, 20, doi: [10.3847/0067-0049/226/2/20](https://doi.org/10.3847/0067-0049/226/2/20)
- Fan, X.-L., & Bai, J.-M. 2016, *ApJ*, 818, 185, doi: [10.3847/0004-637X/818/2/185](https://doi.org/10.3847/0004-637X/818/2/185)
- Fan, Z.-H., & Cao, X. 2004, *ApJ*, 602, 103, doi: [10.1086/380902](https://doi.org/10.1086/380902)
- Fang, T., Canizares, C. R., & Marshall, H. L. 2005, *ApJ*, 633, 61, doi: [10.1086/431749](https://doi.org/10.1086/431749)
- Ferrero, E., Wagner, S. J., Emmanoulopoulos, D., & Ostorero, L. 2006, *A&A*, 457, 133, doi: [10.1051/0004-6361:20065317](https://doi.org/10.1051/0004-6361:20065317)
- Fossati, G., Maraschi, L., Celotti, A., Comastri, A., & Ghisellini, G. 1998, *MNRAS*, 299, 433, doi: [10.1046/j.1365-8711.1998.01828.x](https://doi.org/10.1046/j.1365-8711.1998.01828.x)

- Ghisellini, G., Tavecchio, F., Foschini, L., et al. 2010, *MNRAS*, 402, 497, doi: [10.1111/j.1365-2966.2009.15898.x](https://doi.org/10.1111/j.1365-2966.2009.15898.x)
- Ghisellini, G., Tavecchio, F., & Ghirlanda, G. 2009, *MNRAS*, 399, 2041, doi: [10.1111/j.1365-2966.2009.15397.x](https://doi.org/10.1111/j.1365-2966.2009.15397.x)
- Ghisellini, G., Tagliaferri, G., Foschini, L., et al. 2011, *MNRAS*, 411, 901, doi: [10.1111/j.1365-2966.2010.17723.x](https://doi.org/10.1111/j.1365-2966.2010.17723.x)
- Giommi, P., Capalbi, M., Cavazzuti, E., et al. 2007, *A&A*, 468, 571, doi: [10.1051/0004-6361:20054160](https://doi.org/10.1051/0004-6361:20054160)
- Giommi, P., Polenta, G., Lähteenmäki, A., et al. 2012, *A&A*, 541, A160, doi: [10.1051/0004-6361/201117825](https://doi.org/10.1051/0004-6361/201117825)
- Giommi, P., Perri, M., Capalbi, M., et al. 2021, *MNRAS*, 507, 5690, doi: [10.1093/mnras/stab2425](https://doi.org/10.1093/mnras/stab2425)
- González-Martín, O., & Vaughan, S. 2012, *A&A*, 544, A80, doi: [10.1051/0004-6361/201219008](https://doi.org/10.1051/0004-6361/201219008)
- Gültekin, K., Cackett, E. M., Miller, J. M., et al. 2009, *ApJ*, 706, 404, doi: [10.1088/0004-637X/706/1/404](https://doi.org/10.1088/0004-637X/706/1/404)
- H. E. S. S. Collaboration, Acero, F., Aharonian, F., et al. 2010, *A&A*, 511, A52, doi: [10.1051/0004-6361/200913073](https://doi.org/10.1051/0004-6361/200913073)
- Hardcastle, M. J., Evans, D. A., & Croston, J. H. 2007, *MNRAS*, 376, 1849, doi: [10.1111/j.1365-2966.2007.11572.x](https://doi.org/10.1111/j.1365-2966.2007.11572.x)
- . 2009, *MNRAS*, 396, 1929, doi: [10.1111/j.1365-2966.2009.14887.x](https://doi.org/10.1111/j.1365-2966.2009.14887.x)
- Heinz, S. 2004, *MNRAS*, 355, 835, doi: [10.1111/j.1365-2966.2004.08361.x](https://doi.org/10.1111/j.1365-2966.2004.08361.x)
- Heinz, S., & Sunyaev, R. A. 2003, *MNRAS*, 343, L59, doi: [10.1046/j.1365-8711.2003.06918.x](https://doi.org/10.1046/j.1365-8711.2003.06918.x)
- Ho, L. C. 2002, *ApJ*, 564, 120, doi: [10.1086/324399](https://doi.org/10.1086/324399)
- Hovatta, T., Valtaoja, E., Tornikoski, M., & Lähteenmäki, A. 2009, *A&A*, 494, 527, doi: [10.1051/0004-6361:200811150](https://doi.org/10.1051/0004-6361:200811150)
- Ivezić, Ž., Menou, K., Knapp, G. R., et al. 2002, *AJ*, 124, 2364, doi: [10.1086/344069](https://doi.org/10.1086/344069)
- Kaufmann, S., Wagner, S. J., & Tibolla, O. 2013, *ApJ*, 776, 68, doi: [10.1088/0004-637X/776/2/68](https://doi.org/10.1088/0004-637X/776/2/68)
- Kawakatu, N., Imanishi, M., & Nagao, T. 2007, *ApJ*, 661, 660, doi: [10.1086/516563](https://doi.org/10.1086/516563)
- Keenan, M., Meyer, E. T., Georganopoulos, M., Reddy, K., & French, O. J. 2021, *MNRAS*, 505, 4726, doi: [10.1093/mnras/stab1182](https://doi.org/10.1093/mnras/stab1182)
- Kellermann, K. I., Condon, J. J., Kimball, A. E., Perley, R. A., & Ivezić, Ž. 2016, *ApJ*, 831, 168, doi: [10.3847/0004-637X/831/2/168](https://doi.org/10.3847/0004-637X/831/2/168)
- Kellermann, K. I., Sramek, R., Schmidt, M., Shaffer, D. B., & Green, R. 1989, *AJ*, 98, 1195, doi: [10.1086/115207](https://doi.org/10.1086/115207)
- Körding, E., Falcke, H., & Corbel, S. 2006, *A&A*, 456, 439, doi: [10.1051/0004-6361:20054144](https://doi.org/10.1051/0004-6361:20054144)
- Kovalev, Y. Y., Pushkarev, A. B., Nokhrina, E. E., et al. 2020, *MNRAS*, 495, 3576, doi: [10.1093/mnras/staa1121](https://doi.org/10.1093/mnras/staa1121)
- Li, S.-L., & Gu, M. 2018, *MNRAS*, 481, L45, doi: [10.1093/mnrasl/sly154](https://doi.org/10.1093/mnrasl/sly154)
- . 2021, *A&A*, 654, A141, doi: [10.1051/0004-6361/202141301](https://doi.org/10.1051/0004-6361/202141301)
- Li, Z.-Y., Wu, X.-B., & Wang, R. 2008, *ApJ*, 688, 826, doi: [10.1086/592314](https://doi.org/10.1086/592314)
- Liao, M., Gu, M., Zhou, M., & Chen, L. 2020, *MNRAS*, 497, 482, doi: [10.1093/mnras/staa1559](https://doi.org/10.1093/mnras/staa1559)
- Liu, Y., Jiang, D. R., & Gu, M. F. 2006, *ApJ*, 637, 669, doi: [10.1086/498639](https://doi.org/10.1086/498639)
- Lusso, E., Comastri, A., Vignali, C., et al. 2010, *A&A*, 512, A34, doi: [10.1051/0004-6361/200913298](https://doi.org/10.1051/0004-6361/200913298)
- Magorrian, J., Tremaine, S., Richstone, D., et al. 1998, *AJ*, 115, 2285, doi: [10.1086/300353](https://doi.org/10.1086/300353)
- Malizia, A., Landi, R., Molina, M., et al. 2016, *MNRAS*, 460, 19, doi: [10.1093/mnras/stw972](https://doi.org/10.1093/mnras/stw972)
- Maselli, A., Massaro, E., Nesci, R., et al. 2010, *A&A*, 512, A74, doi: [10.1051/0004-6361/200913343](https://doi.org/10.1051/0004-6361/200913343)
- Mateos, S., Carrera, F. J., Alonso-Herrero, A., et al. 2015, *MNRAS*, 449, 1422, doi: [10.1093/mnras/stv299](https://doi.org/10.1093/mnras/stv299)
- Merloni, A., Heinz, S., & Di Matteo, T. 2003, *MNRAS*, 345, 1057, doi: [10.1046/j.1365-2966.2003.07017.x](https://doi.org/10.1046/j.1365-2966.2003.07017.x)
- Meyer, E. T., Fossati, G., Georganopoulos, M., & Lister, M. L. 2011, *ApJ*, 740, 98, doi: [10.1088/0004-637X/740/2/98](https://doi.org/10.1088/0004-637X/740/2/98)
- Nieppola, E., Tornikoski, M., & Valtaoja, E. 2006, *A&A*, 445, 441, doi: [10.1051/0004-6361:20053316](https://doi.org/10.1051/0004-6361:20053316)
- Nieppola, E., Valtaoja, E., Tornikoski, M., Hovatta, T., & Kotiranta, M. 2008, *A&A*, 488, 867, doi: [10.1051/0004-6361:200809716](https://doi.org/10.1051/0004-6361:200809716)
- Ogle, P. M., Wehrle, A. E., Balonek, T., & Gurwell, M. A. 2011, *ApJS*, 195, 19, doi: [10.1088/0067-0049/195/2/19](https://doi.org/10.1088/0067-0049/195/2/19)
- Padovani, P., Boccardi, B., Falomo, R., & Giommi, P. 2022, *MNRAS*, 511, 4697, doi: [10.1093/mnras/stac376](https://doi.org/10.1093/mnras/stac376)
- Padovani, P., & Giommi, P. 1995, *ApJ*, 444, 567, doi: [10.1086/175631](https://doi.org/10.1086/175631)
- Padovani, P., Perlman, E. S., Landt, H., Giommi, P., & Perri, M. 2003, *ApJ*, 588, 128, doi: [10.1086/373899](https://doi.org/10.1086/373899)
- Padovani, P., Alexander, D. M., Assef, R. J., et al. 2017, *A&A Rv*, 25, 2, doi: [10.1007/s00159-017-0102-9](https://doi.org/10.1007/s00159-017-0102-9)
- Pal, M., Kushwaha, P., Dewangan, G. C., & Pawar, P. K. 2020, *ApJ*, 890, 47, doi: [10.3847/1538-4357/ab65ee](https://doi.org/10.3847/1538-4357/ab65ee)
- Paliya, V. S., Domínguez, A., Ajello, M., Olmo-García, A., & Hartmann, D. 2021, *ApJS*, 253, 46, doi: [10.3847/1538-4365/abe135](https://doi.org/10.3847/1538-4365/abe135)
- Paliya, V. S., Marcotulli, L., Ajello, M., et al. 2017, *ApJ*, 851, 33, doi: [10.3847/1538-4357/aa98e1](https://doi.org/10.3847/1538-4357/aa98e1)
- Paliya, V. S., Ajello, M., Ojha, R., et al. 2019, *ApJ*, 871, 211, doi: [10.3847/1538-4357/aafa10](https://doi.org/10.3847/1538-4357/aafa10)

- Palma, N. I., Böttcher, M., de la Calle, I., et al. 2011, *ApJ*, 735, 60, doi: [10.1088/0004-637X/735/1/60](https://doi.org/10.1088/0004-637X/735/1/60)
- Perlman, E. S., Georganopoulos, M., Marshall, H. L., et al. 2011, *ApJ*, 739, 65, doi: [10.1088/0004-637X/739/2/65](https://doi.org/10.1088/0004-637X/739/2/65)
- Piconcelli, E., Jimenez-Bailón, E., Guainazzi, M., et al. 2005, *A&A*, 432, 15, doi: [10.1051/0004-6361:20041621](https://doi.org/10.1051/0004-6361:20041621)
- Piner, B. G., Pant, N., & Edwards, P. G. 2008, *ApJ*, 678, 64, doi: [10.1086/533521](https://doi.org/10.1086/533521)
- Plotkin, R. M., Markoff, S., Kelly, B. C., Körding, E., & Anderson, S. F. 2012, *MNRAS*, 419, 267, doi: [10.1111/j.1365-2966.2011.19689.x](https://doi.org/10.1111/j.1365-2966.2011.19689.x)
- Raiteri, C. M., Villata, M., Kadler, M., et al. 2006, *A&A*, 452, 845, doi: [10.1051/0004-6361:20054409](https://doi.org/10.1051/0004-6361:20054409)
- Raiteri, C. M., Villata, M., Capetti, A., et al. 2009, *A&A*, 507, 769, doi: [10.1051/0004-6361/200912953](https://doi.org/10.1051/0004-6361/200912953)
- Rakshit, S., Stalin, C. S., & Kotilainen, J. 2020, *ApJS*, 249, 17, doi: [10.3847/1538-4365/ab99c5](https://doi.org/10.3847/1538-4365/ab99c5)
- Readhead, A. C. S., Ravi, V., Liodakis, I., et al. 2021, *ApJ*, 907, 61, doi: [10.3847/1538-4357/abd08c](https://doi.org/10.3847/1538-4357/abd08c)
- Ricci, C., Ueda, Y., Ichikawa, K., et al. 2014, *A&A*, 567, A142, doi: [10.1051/0004-6361/201322701](https://doi.org/10.1051/0004-6361/201322701)
- Ricci, C., Trakhtenbrot, B., Koss, M. J., et al. 2017, *ApJS*, 233, 17, doi: [10.3847/1538-4365/aa96ad](https://doi.org/10.3847/1538-4365/aa96ad)
- Sambruna, R. M., Donato, D., Cheung, C. C., Tavecchio, F., & Maraschi, L. 2008, *ApJ*, 684, 862, doi: [10.1086/589918](https://doi.org/10.1086/589918)
- Saxton, R. D., Read, A. M., Esquej, P., et al. 2008, *A&A*, 480, 611, doi: [10.1051/0004-6361:20079193](https://doi.org/10.1051/0004-6361:20079193)
- Sbarrato, T., Ghisellini, G., Maraschi, L., & Colpi, M. 2012, *MNRAS*, 421, 1764, doi: [10.1111/j.1365-2966.2012.20442.x](https://doi.org/10.1111/j.1365-2966.2012.20442.x)
- Scarpa, R., & Falomo, R. 1997, *A&A*, 325, 109
- Shaw, M. S., Romani, R. W., Cotter, G., et al. 2012, *ApJ*, 748, 49, doi: [10.1088/0004-637X/748/1/49](https://doi.org/10.1088/0004-637X/748/1/49)
- Shen, Y., Richards, G. T., Strauss, M. A., et al. 2011, *ApJS*, 194, 45, doi: [10.1088/0067-0049/194/2/45](https://doi.org/10.1088/0067-0049/194/2/45)
- Shi, Y., Rieke, G. H., Hines, D. C., et al. 2005, *ApJ*, 629, 88, doi: [10.1086/431344](https://doi.org/10.1086/431344)
- Shinozaki, K., Miyaji, T., Ishisaki, Y., Ueda, Y., & Ogasaka, Y. 2006, *AJ*, 131, 2843, doi: [10.1086/504155](https://doi.org/10.1086/504155)
- Sikora, M., Stawarz, L., & Lasota, J.-P. 2007, *ApJ*, 658, 815, doi: [10.1086/511972](https://doi.org/10.1086/511972)
- Tavecchio, F., Ghisellini, G., Ghirlanda, G., Foschini, L., & Maraschi, L. 2010, *MNRAS*, 401, 1570, doi: [10.1111/j.1365-2966.2009.15784.x](https://doi.org/10.1111/j.1365-2966.2009.15784.x)
- Torrealba, J., Chavushyan, V., Cruz-González, I., et al. 2012, *RMxAA*, 48, 9, doi: [10.48550/arXiv.1107.3416](https://doi.org/10.48550/arXiv.1107.3416)
- Torresi, E., Grandi, P., Capetti, A., Baldi, R. D., & Giovannini, G. 2018, *MNRAS*, 476, 5535, doi: [10.1093/mnras/sty520](https://doi.org/10.1093/mnras/sty520)
- Ueda, Y., Ishisaki, Y., Takahashi, T., Makishima, K., & Ohashi, T. 2001, *ApJS*, 133, 1, doi: [10.1086/319189](https://doi.org/10.1086/319189)
- . 2005, *ApJS*, 161, 185, doi: [10.1086/468187](https://doi.org/10.1086/468187)
- Urry, C. M., & Padovani, P. 1995, *PASP*, 107, 803, doi: [10.1086/133630](https://doi.org/10.1086/133630)
- Vestergaard, M., & Osmer, P. S. 2009, *ApJ*, 699, 800, doi: [10.1088/0004-637X/699/1/800](https://doi.org/10.1088/0004-637X/699/1/800)
- Wang, J.-M., Luo, B., & Ho, L. C. 2004, *ApJL*, 615, L9, doi: [10.1086/426060](https://doi.org/10.1086/426060)
- Wang, R., Wu, X.-B., & Kong, M.-Z. 2006, *ApJ*, 645, 890, doi: [10.1086/504401](https://doi.org/10.1086/504401)
- Wang, S., Liu, J., Qiu, Y., et al. 2016, *ApJS*, 224, 40, doi: [10.3847/0067-0049/224/2/40](https://doi.org/10.3847/0067-0049/224/2/40)
- Wang, Y., Wang, T., Ho, L. C., Zhong, Y., & Luo, B. 2024, *A&A*, 689, A327, doi: [10.1051/0004-6361/202449732](https://doi.org/10.1051/0004-6361/202449732)
- Warwick, R. S., Saxton, R. D., & Read, A. M. 2012, *A&A*, 548, A99, doi: [10.1051/0004-6361/201118642](https://doi.org/10.1051/0004-6361/201118642)
- Woo, J.-H., & Urry, C. M. 2002, *ApJ*, 579, 530, doi: [10.1086/342878](https://doi.org/10.1086/342878)
- Woo, J.-H., Urry, C. M., van der Marel, R. P., Lira, P., & Maza, J. 2005, *ApJ*, 631, 762, doi: [10.1086/432681](https://doi.org/10.1086/432681)
- Wu, X.-B., Liu, F. K., & Zhang, T. Z. 2002, *A&A*, 389, 742, doi: [10.1051/0004-6361:20020577](https://doi.org/10.1051/0004-6361:20020577)
- Wu, Z., Jiang, D., Gu, M., & Chen, L. 2014, *A&A*, 562, A64, doi: [10.1051/0004-6361/201220851](https://doi.org/10.1051/0004-6361/201220851)
- Wu, Z., Jiang, D. R., Gu, M., & Liu, Y. 2007, *A&A*, 466, 63, doi: [10.1051/0004-6361:20066754](https://doi.org/10.1051/0004-6361:20066754)
- Wu, Z.-Z., Gu, M.-F., & Jiang, D.-R. 2009, *RA&A*, 9, 168, doi: [10.1088/1674-4527/9/2/006](https://doi.org/10.1088/1674-4527/9/2/006)
- Xie, F.-G., & Yuan, F. 2017, *ApJ*, 836, 104, doi: [10.3847/1538-4357/aa5b90](https://doi.org/10.3847/1538-4357/aa5b90)
- Xiong, D., Zhang, X., Bai, J., & Zhang, H. 2015, *MNRAS*, 450, 3568, doi: [10.1093/mnras/stv812](https://doi.org/10.1093/mnras/stv812)
- Xu, Y.-D., Cao, X., & Wu, Q. 2009, *ApJL*, 694, L107, doi: [10.1088/0004-637X/694/2/L107](https://doi.org/10.1088/0004-637X/694/2/L107)
- Yang, J. H., Fan, J. H., Liu, Y., et al. 2022a, *ApJS*, 262, 18, doi: [10.3847/1538-4365/ac7deb](https://doi.org/10.3847/1538-4365/ac7deb)
- Yang, W. X., Wang, H. G., Liu, Y., et al. 2022b, *ApJ*, 925, 120, doi: [10.3847/1538-4357/ac3a09](https://doi.org/10.3847/1538-4357/ac3a09)
- Ye, X.-H., & Fan, J.-H. 2021, *PASJ*, 73, 775, doi: [10.1093/pasj/psab039](https://doi.org/10.1093/pasj/psab039)
- Yuan, F., & Cui, W. 2005, *ApJ*, 629, 408, doi: [10.1086/431453](https://doi.org/10.1086/431453)
- Yuan, F., Yu, Z., & Ho, L. C. 2009, *ApJ*, 703, 1034, doi: [10.1088/0004-637X/703/1/1034](https://doi.org/10.1088/0004-637X/703/1/1034)
- Yuan, Z., & Wang, J. 2012, *ApJ*, 744, 84, doi: [10.1088/0004-637X/744/2/84](https://doi.org/10.1088/0004-637X/744/2/84)
- Zhang, L., Fan, J., & Zhu, J. 2021, *PASJ*, 73, 313, doi: [10.1093/pasj/psaa122](https://doi.org/10.1093/pasj/psaa122)

Zhang, X., Xiong, D.-r., Gao, Q.-g., et al. 2024, MNRAS,
529, 3699, doi: [10.1093/mnras/stae765](https://doi.org/10.1093/mnras/stae765)

Zhu, S. F., Brandt, W. N., Luo, B., et al. 2020, MNRAS,
496, 245, doi: [10.1093/mnras/staa1411](https://doi.org/10.1093/mnras/staa1411)

Table 2. The properties of Blazars

IAU Name	z	$\log \nu_{\text{peak}}$	Type	δ	Γ	$\log L_{X,\text{obs}}$	$\log L_{X,\text{int}}$	$\log L_{R,\text{obs}}$	$\log L_{R,\text{int}}$	$\log M_{\text{HB,dyn}}$	Refs.	$\log R$	$\log \lambda_{\text{int}}$
(1)	(2)	(3)	(4)	(5)	(6)	(7)	(8)	(9)	(10)	(11)	(12)	(13)	(14)
0007+106	0.089	14.88	ISF	1.77	1.75	44.143	43.916	41.176	40.680	8.29	1, 2	1.81	-2.488
0106+013	2.099	12.51	LSF	21.61	1.45	46.626	45.536	45.819	43.150	9.51	3, 4	4.53	-2.088
0133+476	0.859	12.66	LSF	24.47	1.40	45.979	44.868	44.717	41.940	8.73	5, 6	3.56	-1.976
0149+218	1.320	12.80	LSF	5.77	1.69	45.640	44.958	44.424	42.902	8.83	3, 7	4.06	-1.986
0212+735	2.367	12.14	LSF	9.57	1.51	47.407	46.587	45.745	43.784	9.58	8, 9	4.62	-1.107
0234+285	1.213	12.76	LSF	19.89	1.40	46.239	45.200	44.963	42.366	9.22	3, 10	4.53	-2.134
0306+102	0.863	12.76	LSF	14.13	1.65	45.715	44.699	44.086	41.786	7.77	3, 9	3.68	-1.185
0333+321	1.263	13.16	LSF	26.34	1.57	46.845	45.628	45.208	42.367	9.25	11, 12	3.93	-1.736
0355+508	1.510	12.54	LSF	15.93	1.47	46.913	45.923	45.884	43.480	9.67	8, 13	3.30	-1.860
0420-014	0.915	12.77	LSF	24.98	2.10	46.053	44.608	44.935	42.140	9.03	14, 6	4.30	-2.536
0440-003	0.844	12.29	LSF	14.86	1.73	45.612	44.545	44.594	42.250	8.81	3, 15	4.05	-2.379
0458-020	2.286	12.70	LSF	19.49	1.52	46.585	45.502	45.342	42.762	8.66	16, 9	3.89	-1.272
0528+134	2.070	12.13	LSF	37.72	1.58	46.593	45.237	45.853	42.700	9.80	17, 18	4.81	-2.677
0552+398	2.363	11.54	LSF	32.21	1.63	46.808	45.486	46.080	43.064	9.74	8, 19	4.55	-2.368
0605-085	0.872	12.13	LSF	8.87	1.42	45.815	45.050	44.291	42.396	8.98	3, 9	3.63	-2.043
0642+449	3.396	13.03	LSF	12.20	1.49	46.918	46.016	46.186	44.014	9.12	3,	4.72	-1.218
0736+017	0.191	13.18	LSF	9.68		44.579	43.731	42.963	40.990	8.00	20, 6	3.38	-2.383
0804+499	1.436	11.99	LSF	43.23	1.69	46.103	44.637	44.695	41.423	8.84	3, 21	2.20	-2.317
0827+243	0.941	12.53	LSF	15.93	1.46	45.721	44.735	44.587	42.183	9.01	22, 21	3.41	-2.389
0836+710	2.218	13.47	LSF	20.15	1.46	47.785	46.715	45.867	43.258	10.20	8, 9	3.86	-1.599
0847-120	0.566	13.11	LSF	20.29	1.66	44.949	43.790	43.644	41.030	9.07	3, 9	3.96	-3.394
0923+392	0.695	12.64	LSF	4.80		45.976	45.389	44.468	43.105	9.28	20, 6	3.63	-2.005
0945+408	1.249	12.34	LSF	7.37	1.54	45.858	45.124	44.763	43.028	8.95	3, 21	3.62	-1.940
0953+254	0.712	12.66	LSF	4.80	1.66	45.366	44.762	44.224	42.861	8.63	3, 21	2.47	-1.982
1156+295	0.729	13.07	LSF	34.29	1.52	45.623	44.333	44.255	41.185	8.89	5, 9	3.42	-2.761
1222+216	0.432	13.46	LSF	5.89	2.12	45.316	44.515	43.219	41.678	8.87	8, 21	2.48	-2.469
1226+023	0.158	13.85	LSF	19.88	1.60	45.733	44.608	43.957	41.361	8.69	23, 9	2.99	-2.196

Table 2 continued

Table 2 (continued)

IAU Name	z	$\log \nu_{\text{peak}}$	Type	δ	Γ	$\log L_{X,\text{obs}}$	$\log L_{X,\text{int}}$	$\log L_{R,\text{obs}}$	$\log L_{R,\text{int}}$	$\log M_{\text{HB,dyn}}$	Refs.	$\log R$	$\log \lambda_{\text{int}}$
(1)	(2)	(3)	(4)	(5)	(6)	(7)	(8)	(9)	(10)	(11)	(12)	(13)	(14)
1253-055	0.536	12.71	LSF	30.56	1.57	46.211	44.939	44.827	41.857	8.63	24, 9	4.64	-1.805
1324+224	1.400	12.48	LSF	25.09	1.49	46.167	45.005	44.780	41.981	9.24	3, 21	3.52	-2.348
1502+106	1.839	12.70	LSF	14.50	1.32	46.269	45.371	44.841	42.518	9.13	25, 9	3.45	-1.873
1510-089	0.360	13.04	LSF	20.69	1.40	45.294	44.242	43.558	40.926	8.65	5, 6	3.51	-2.522
1606+106	1.226	12.99	LSF	29.86	1.31	46.094	44.958	44.783	41.833	8.77	3, 10	3.74	-1.926
1611+343	1.401	12.26	LSF	16.72	1.58	46.035	44.983	45.326	42.880	9.08	3, 10	4.04	-2.211
1633+382	1.814	12.47	LSF	25.47	1.46	46.992	45.839	45.495	42.683	9.53	26, 21	3.97	-1.805
1637+574	0.751	12.80	LSF	16.20	1.82	45.573	44.436	44.214	41.795	8.69	3, 9	3.22	-2.368
1641+399	0.593	13.01	LSF	9.12	1.76	45.728	44.845	44.800	42.880	8.88	8, 10	4.37	-2.149
1725+044	0.293	13.46	LSF	4.09	1.58	44.545	44.019	43.132	41.909	8.07	3, 6	3.48	-2.165
1730-130	0.902	12.63	LSF	12.81	1.61	45.786	44.823	45.094	42.879	8.45	27, 9	5.01	-1.741
1739+522	1.375	13.12	LSF	31.75	1.84	46.778	45.487	45.057	42.054	9.09	28, 9	4.00	-1.717
1741-038	1.054	12.72	LSF	23.22	1.35	46.111	45.041	45.010	42.279	9.29	27, 29	5.15	-2.363
1828+487	0.692	12.99	LSF	6.51	1.32	45.731	45.102	44.689	43.062	8.59	30, 31	3.93	-1.602
1928+738	0.302	13.33	LSF	1.79	1.84	45.221	44.942	42.825	42.236	8.91	8, 6	2.38	-2.082
2121+053	1.941	12.63	LSF	17.79	1.95	46.338	45.109	45.487	42.987	9.33	3, 9	3.98	-2.335
2134+004	1.932	12.92	LSF	18.77	1.71	46.789	45.639	45.829	43.282	9.53	11, 21	3.97	-2.005
2145+067	0.990	12.53	LSF	19.22	1.52	46.404	45.326	44.846	42.278	8.87	8, 32	3.45	-1.658
2201+315	0.295	13.24	LSF	7.44	1.79	45.069	44.258	43.294	41.551	8.87	33, 6	2.86	-2.726
2227-088	1.562	12.68	LSF	18.52	1.34	47.137	46.046	45.236	42.700	8.96	28, 21	4.01	-1.028
2230+114	1.037	12.47	LSF	19.22	1.34	46.305	45.303	45.283	42.715	9.09	8, 9	4.31	-1.901
2234+282	0.795	12.96	LSF	6.62	1.52	45.479	44.789	44.472	42.830	8.44	3, 9	3.98	-1.765
2251+158	0.859	13.11	LSF	43.33	1.53	46.333	44.952	45.354	42.081	9.17	34, 6	3.92	-2.332
0003-066	0.347	12.92	LBL	5.40	1.67	44.647	43.996	43.579	42.115	8.93	3, 9	4.34	-3.048
0059+581	0.664	12.67	LBL	17.86	1.79	45.277	44.146	44.154	41.651	9.01	35, 9	4.63	-2.978
0138-097	0.733	13.24	LBL	5.90	1.79	45.733	45.037	43.940	42.398	9.84	36, 37	3.08	-2.917
0208-512	0.999	12.94	LBL	3.27	1.72	46.288	45.821	43.799	42.770	9.12	38, 9	3.05	-1.413
0214+083	1.400	13.56	LBL	6.60	1.69	46.186	45.451	44.269	42.630	8.40	3, 9	2.78	-1.063
0235+164	0.940	13.03	LBL	10.78	1.82	45.800	44.830	44.353	42.288	9.07	39, 18	3.53	-2.357
0336-019	0.850	12.67	LBL	5.12	1.82	45.390	44.750	44.310	42.891	8.98	40, 6	3.31	-2.344

Table 2 continued

Table 2 (continued)

IAU Name	z	$\log \nu_{\text{peak}}$	Type	δ	Γ	$\log L_{X,\text{obs}}$	$\log L_{X,\text{int}}$	$\log L_{R,\text{obs}}$	$\log L_{R,\text{int}}$	$\log M_{\text{HB,dyn}}$	Refs.	$\log R$	$\log \lambda_{\text{int}}$
(1)	(2)	(3)	(4)	(5)	(6)	(7)	(8)	(9)	(10)	(11)	(12)	(13)	(14)
0422+004	0.310	13.67	LBL	18.37		44.847	43.705	43.364	40.835	8.76	35, 9	2.11	-3.169
0426-380	1.110	12.68	LBL	6.18*	1.93	45.692	44.920	44.379	42.797	8.77	41, 9	3.49	-1.964
0430+289	0.970	12.31	LBL	6.00*	1.42	45.050	44.422	43.830	42.273	8.25	3, 9	3.85	-1.942
0521-365	0.055	13.63	LBL	3.08	1.76	43.531	43.081	42.052	41.075	7.79	42, 9	2.97	-2.823
0723-008	0.128	12.90	LBL	1.79	1.56	44.280	44.065	41.684	41.179	8.00	8, 9	2.59	-2.049
0735+178	0.424	13.44	LBL	11.03	1.56	44.665	43.775	43.802	41.716	8.30	14, 18	2.54	-2.639
0749+540	0.200	12.56	LBL	5.50	1.79	43.656	42.968	42.631	41.150	8.94	3,	3.80	-4.086
0754+100	0.266	12.89	LBL	8.10	1.59	44.846	44.062	43.080	41.263	8.53	3, 9	2.67	-2.582
0808+019	1.148	12.52	LBL	12.30	1.66	45.373	44.407	43.210	42.030	8.71	3, 9	2.76	-2.417
0814+425	0.530	13.01	LBL	6.33	1.76	44.530	43.793	43.757	42.154	8.01	14, 43	3.63	-2.331
0820+225	0.951	13.09	LBL	3.00		45.125	44.694	43.297	42.343	7.96	44, 9	2.37	-1.380
0823+033	0.506	13.04	LBL	29.41	1.73	45.045	43.709	43.865	40.928	8.55	3, 43	2.91	-2.955
0828+493	0.548	12.92	LBL	8.39		44.865	43.030	43.255	41.408	8.69	36, 45	3.82	-2.773
0829+046	0.174	13.70	LBL	5.28	1.50	44.056	43.453	42.437	40.991	8.46	3, 46	2.35	-3.121
0829+089	0.941	13.66	LBL	4.04	1.84	45.537	44.963	43.152	41.939	8.73	3, 21	2.72	-1.881
0851+202	0.306	13.24	LBL	14.76	1.96	44.907	43.754	43.420	41.082	8.79	47, 29	2.54	-3.150
0954+658	0.367	13.07	LBL	4.37		45.100	44.521	43.174	41.893	8.53	48, 15	3.54	-2.123
0958+294	0.558	12.97	LBL	5.76	1.76	45.083	44.384	42.958	41.438	7.78	3, 9	3.22	-1.510
1055+018	0.894	12.87	LBL	8.56*	1.80	45.868	44.997	44.733	42.868	9.50	5, 9	4.07	-2.617
1057-797	0.581	12.72	LBL	11.77*	1.90	45.264	44.229	44.162	42.020	8.64	5, 9	3.99	-2.525
1144-379	1.048	12.60	LBL	17.72	1.96	45.447	44.216	44.822	42.326	8.69	5, 9	4.03	-2.588
1308+326	0.996	12.72	LBL	27.73	1.60	45.985	44.734	44.752	41.866	8.81	5, 21	4.61	-2.190
1404+286	0.077	13.25	LBL	2.72	2.21	43.950	43.485	41.860	40.991	8.73	49, 7	2.75	-3.359
1413+135	0.247	12.82	LBL	13.18	1.59	44.100	43.133	43.004	40.764	7.88	49, 50	4.67	-2.861
1418+546	0.153	13.68	LBL	8.31	1.88	43.709	42.826	42.530	40.690	9.03	11, 6	2.97	-4.318
1501+481	0.345	13.12	LBL	1.96		43.649	43.385	41.306	40.722	7.97	51, 9	2.02	-2.699
1514-241	0.049	13.96	LBL	11.69	1.60	43.245	42.420	41.862	39.726	8.10	52, 6	2.81	-3.794
1519-273	1.294	12.72	LBL	22.33	2.25	45.713	44.251	45.072	42.375	8.80	11, 53	4.07	-2.663
1538+149	0.605	13.33	LBL	9.46	1.77	45.005	44.104	44.018	42.066	8.94	3, 29	3.49	-2.950
1622-253	0.786	12.62	LBL	7.15	0.72	45.704	45.214	44.237	42.528	7.70	14, 9	5.03	-0.600

Table 2 continued

Table 2 (continued)

IAU Name	z	$\log \nu_{\text{peak}}$	Type	δ	Γ	$\log L_{X,\text{obs}}$	$\log L_{X,\text{int}}$	$\log L_{R,\text{obs}}$	$\log L_{R,\text{int}}$	$\log M_{\text{HB,dyn}}$	Refs.	$\log R$	$\log \lambda_{\text{int}}$
(1)	(2)	(3)	(4)	(5)	(6)	(7)	(8)	(9)	(10)	(11)	(12)	(13)	(14)
1749+096	0.322	12.90	LBL	37.10	1.93	44.952	43.420	43.816	40.677	7.98	14, 9	4.14	-2.674
1803+784	0.684	13.25	LBL	8.51	1.50	45.579	44.804	44.297	42.437	8.94	5, 9	3.47	-2.250
1807+698	0.051	13.89	LBL	3.78	1.30	42.937	42.494	41.672	40.517	8.49	54, 46	2.31	-4.110
1823+568	0.663	13.16	LBL	4.07	1.61	45.503	44.972	43.924	42.704	9.26	26, 45	3.54	-2.401
2007+777	0.342	13.38	LBL	7.92	1.98	44.690	43.797	43.213	41.415	7.50	55, 45	3.20	-1.816
2029+121	1.215	12.56	LBL	8.94	1.53	45.376	44.573	44.647	42.744	8.31	3, 9	3.91	-1.851
2131-021	1.285	12.92	LBL	16.75	1.66	45.952	44.867	44.477	42.029	8.75	3, 9	3.69	-1.997
2150+173	0.871	13.36	LBL	6.60	1.12	45.040	44.461	44.118	42.479	8.61	3, 9	3.57	-2.263
2200+420	0.069	13.59	LBL	9.13	1.91	43.994	43.063	42.062	40.141	8.23	56, 6	1.99	-3.281
2209+236	1.125	11.92	LBL	21.19		45.474	44.276	44.194	41.542	8.69	57, 9	4.10	-2.527
2214+241	0.505	13.04	LBL	5.17	1.86	44.718	44.038	43.324	41.897	8.44	3, 9	3.35	-2.516
2223-052	1.404	12.96	LBL	19.11		47.011	45.853	45.575	43.012	8.81	28, 29	4.68	-1.071
2240-260	0.774	13.60	LBL	6.08*	1.92	44.804	44.041	43.898	42.331	8.47	3, 9	3.52	-2.543
2254+074	0.190	12.79	LBL	7.11		43.666	42.896	42.370	40.667	8.62	NED, 6	2.66	-3.838
0048-097	0.634	14.12	IBL	8.46	1.96	45.389	44.474	43.890	42.035	8.85	11, 9	2.70	-2.490
0118-272	0.559	14.15	IBL	9.81	2.33	44.771	43.671	43.636	41.653	9.54	3, 37	2.67	-3.983
0607+710	0.267	14.60	IBL	2.50	2.99	43.814	43.285	41.127	40.331	8.87	58, 43	1.45	-3.699
0716+714	0.310	14.17	IBL	10.03	2.72	45.170	43.928	43.589	41.586	8.10	59, 18	2.43	-2.286
1053+494	0.140	15.29	IBL	2.49	2.30	43.147	42.711	41.023	40.230	9.03	61, 43	1.87	-4.433
1055+567	0.143	14.75	IBL	3.55	2.53	43.959	43.312	41.691	40.591	8.33	3, 9	1.86	-3.132
1215+303	0.130	15.21	IBL	3.72	2.53	43.922	43.251	41.901	40.760	8.12	61, 6	1.83	-2.983
1219+285	0.102	14.65	IBL	8.69	2.79	43.854	42.668	42.096	40.218	8.55	62, 9	2.21	-3.996
1222+488	0.647	14.66	IBL	3.56		44.565	43.923	42.265	40.162	8.91	NED, 21	2.18	-3.091
1246+586	0.847	14.88	IBL	5.79	2.53	45.457	44.560	43.697	42.172	9.15	14, 43	2.22	-2.704
1424+240	0.160	15.29	IBL	4.23	2.35	44.150	43.450	41.946	40.693	8.79	14, 63	1.66	-3.453
1458+224	0.235	14.82	IBL	3.38	2.62	44.067	43.429	41.699	40.642	8.81	27, 9	1.99	-3.495
1532+302	0.064	14.27	IBL	1.66		42.840	42.588	40.367	39.927	8.27	64, 9	1.36	-3.796
1532+372	0.143	14.20	IBL	2.22		43.596	43.199	40.742	40.049	7.83	36, 9	1.81	-2.745
1749+701	0.770	14.10	IBL	12.20	2.01	45.510	44.420	44.394	42.221	9.90	3, 43	3.36	-3.594
1914-194	0.137	15.05	IBL	3.69	2.24	43.427	42.815	41.867	40.733	8.90	3, 65	2.37	-4.199

Table 2 continued

Table 2 (continued)

IAU Name	z	$\log \nu_{\text{peak}}$	Type	δ	Γ	$\log L_{X,\text{obs}}$	$\log L_{X,\text{int}}$	$\log L_{R,\text{obs}}$	$\log L_{R,\text{int}}$	$\log M_{\text{HB,dyn}}$	Refs.	$\log R$	$\log \lambda_{\text{int}}$
(1)	(2)	(3)	(4)	(5)	(6)	(7)	(8)	(9)	(10)	(11)	(12)	(13)	(14)
2005-489	0.071	15.30	IBL	2.50	2.31	44.353	43.914	41.447	40.651	9.03	66, 6	1.86	-3.230
2201+044	0.028	14.44	IBL	1.37		42.114	41.957	40.179	39.906	8.10	44, 6	2.08	-4.256

NOTE—Col. (1) Name; Col. (2) Redshift; Col. (3) The synchrotron-peak frequency of blazars (Hz); Col. (4) The Type of blazars, LSF (ISF) indicate low (intermediate)-synchrotron-peaked FSRQ, LBL (IBL) indicate low (intermediate)-synchrotron-peaked BL Lac; Col. (5) The 5 GHz Doppler factor (“**”) indicate that the 5 GHz Doppler factors are estimated by us; Col. (6) The power law photon index; Col. (7) Logarithm of the observational 2–10 keV X-ray luminosity ($\text{erg} \cdot \text{s}^{-1}$); Col. (8) Logarithm of the intrinsic 2–10 keV X-ray luminosity that are corrected from $L_{X,\text{obs}}$ using the Doppler factor ($\text{erg} \cdot \text{s}^{-1}$); Col. (9) Logarithm of the observational 5 GHz core radio luminosity ($\text{erg} \cdot \text{s}^{-1}$); Col. (10) Logarithm of the intrinsic 5 GHz core radio luminosity that are corrected from $L_{R,\text{obs}}$ using the Doppler factor ($\text{erg} \cdot \text{s}^{-1}$); Col. (11) Logarithm of black hole mass (M_{\odot}); Col. (12) References for X-ray data and BH mass; Col. (13) Logarithm of radio-loudness; Col. (14) Eddington-ratio: $\lambda_{\text{int}} = \log(L_{X,\text{int}}/L_{\text{Edd}})$.

References: (1) Shinozaki et al. (2006); (2) Kawakatu et al. (2007); (3) Paliya et al. (2017); (4) Vestergaard & Osmer (2009); (5) Ghisellini et al. (2010); (6) Woo & Urry (2002); (7) Rakshit et al. (2020); (8) Ricci et al. (2017); (9) Paliya et al. (2021); (10) Shaw et al. (2012); (11) Donato et al. (2005); (12) Liu et al. (2006); (13) Acosta-Pulido et al. (2010); (14) Giommi et al. (2012); (15) Fan & Cao (2004); (16) Ghisellini et al. (2011); (17) Palma et al. (2011); (18) Zhang et al. (2024); (19) Paliya et al. (2019); (20) Ueda et al. (2005); (21) Shen et al. (2011); (22) Abdo et al. (2010); (23) Piconcelli et al. (2005); (24) Fang et al. (2005); (25) Cerruti et al. (2011); (26) Giommi et al. (2021); (27) Malizia et al. (2016); (28) Warwick et al. (2012); (29) Wang et al. (2004); (30) Shi et al. (2005); (31) Kovalev et al. (2020); (32) Liu et al. (2006); (33) Ricci et al. (2014); (34) Ogle et al. (2011); (35) Saxton et al. (2008); (36) Dwelly et al. (2017); (37) Xu et al. (2009); (38) Perlman et al. (2011); (39) Raiteri et al. (2006); (40) Bhattacharya et al. (2013); (41) Ghisellini et al. (2009); (42) Boissay et al. (2016); (43) Wu et al. (2009); (44) Wang et al. (2016); (45) Wu et al. (2002); (46) Woo et al. (2005); (47) Pal et al. (2020); (48) González-Martín & Vaughan (2012); (49) Liao et al. (2020); (50) Readhead et al. (2021); (51) Ueda et al. (2001); (52) Kaufmann et al. (2013); (53) Sbarrato et al. (2012); (54) Torresi et al. (2018); (55) Sambruna et al. (2008); (56) Raiteri et al. (2009); (57) Giommi et al. (2007); (58) Carrera et al. (2007); (59) Ferrero et al. (2006); (60) Tavecchio et al. (2010); (61) Aleksić et al. (2012); (62) Acciari et al. (2009); (63) Padovani et al. (2022); (64) Mateos et al. (2015); (65) Carangelo et al. (2003); (66) H. E. S. S. Collaboration et al. (2010).